The Climatology of Relative Humidity in the Atmosphere

JOSÉ P. PEIXOTO

University of Lisbon, Lisbon, Portugal

ABRAHAM H. OORT

Geophysical Fluid Dynamics Laboratory/NOAA, Princeton, New Jersey

(Manuscript received 11 August 1995, in final form 24 May 1996)

ABSTRACT

The present paper deals with the analysis of the time-average relative humidity fields in the atmosphere. Twice-daily estimates of relative humidity are used.

After some theoretical considerations on the relations between relative humidity, other moisture parameters, and temperature, a critical analysis of the various sources of data is made considering their possible limitations. Various methods of computing relative humidity are formulated and discussed.

The global distribution of relative humidity at various levels shows that it is not zonally uniform with centers of various intensities at all latitudes. The global maps show maxima in the equatorial zone and minima in the dry subtropical belts around 30°N and 30°S. The land–sea contrast and variations related to the orographic relief are also apparent. The general pattern of relative humidity is similar at all levels but its magnitude decreases with altitude. The seasonal analyses show a similar pattern as the annual analyses but are slightly shifted toward the summer pole.

The saturation deficit is also evaluated. Cross sections of the saturation deficit show that the maxima are found in the middle to lower troposphere at subtropical latitudes, being most intense in the Northern Hemisphere during the summer season.

The temporal variability of the relative humidity due to transient eddies exhibits a bimodal structure with maxima in the midlatitudes of each hemisphere around 700 mb. The stationary eddy distributions are less pronounced than the transient ones and do not change substantially from one season to another.

To validate our results, several comparisons are made using independent sources of humidity data as well as cloud distributions at various levels. Thus, COADS data are used to obtain independent analyses of the surface relative humidity over the oceans, and satellite observations by SAGE are used at the 300-mb level. The rawinsonde-SAGE differences are on the order of 10% in the Tropics and 20% in the high latitudes, due in part to a clear-sky (dry) bias in the SAGE data. Our results are further compared with those obtained from operational analyses by the ECMWF. The differences do not exceed 5% in the Tropics but tend to be larger in the tropical upper troposphere and at all levels in the extratropics of the Southern Hemisphere, where the radiosonde network is quite sparse. In view of the obvious connections between the moisture distribution in the atmosphere and cloudiness, a cloud climatology is used to check its consistency with the present results. The latitudinal and interseasonal variations of cloudiness and relative humidity are similar, with maxima in the equatorial belt and at high latitudes and minima in the subtropics that shift poleward during summer and equatorward during winter.

Finally, some comments are made on the radiosonde-observing systems in the light of recent satellite studies of humidity. Mainly at the upper levels systematic localized differences are found between electrical hygristor and organic sensors, but the differences almost disappear in the middle and lower troposphere.

In spite of the shortcomings, limitations, and errors of the radiosonde network, the present analyses describe for the first time the large-scale, three-dimensional characteristics of the relative humidity in the global atmosphere.

1. Introduction

The present study deals with the climatology of relative humidity in the atmosphere based on radiosonde data for the period May 1973–April 1988. Around the year 1973, the radiosonde instrumentation had improved (mainly in the United States) to a satisfactory level to guarantee the needed precision of the data in the mid- and low troposphere. However, important instrument changes have taken place in Europe, Australia, South America, and Africa since 1973 (Gaffen 1993). Relative humidity studies on a global scale have not been very numerous but some studies are worth mentioning. First is a pioneering study by Szava-Kovats (1938), who presented surface maps of mean relative humidity and mean water vapor pressure for January and July conditions. For the upper atmosphere,

Corresponding author address: Dr. Abraham H. Oort, GFDL/NOAA, Princeton University, Forrestal Campus, US Route 1, Post Office Box 308, Princeton, NJ 08542.

however, the research on relative humidity has been mainly confined to regional studies with the notable exception of studies by Telegadas and London (1954) and more recently Gaffen et al. (1992). Telegadas and London presented maps for the Northern Hemisphere at 850, 700, and 500 mb based on a 2-yr average using around 150 upper-air stations available at the time. Gaffen et al. (1992) studied various relative humidity regimes around the world based on 56 selected radiosonde stations for the period 1973–90. Rasmusson (1972) and Rind et al. (1991) have presented cross sections of the seasonal variations of relative humidity.

Relative humidity is the quantity most used for general applications, such as in agriculture, hydrology, management of water resources, human comfort, etc. It is the decisive factor that, besides the wind speed, determines the amount and rate of evaporation, and it constitutes therefore a critical factor to evaluate the rate of loss of moisture by soil, plants, water reservoirs, etc.

Relative humidity differs both qualitatively and quantitatively from other moisture parameters. It can be altered either by changing the amount of water vapor in the atmosphere (e.g., through evaporation) or by varying the holding capacity of the air for moisture (e.g., by changing the temperature).

A moist atmosphere can be regarded as a system with two components, dry air and water substance. We will use the Gibbs' phase rule, which states that the number of degrees of freedom l is equal to the difference between the number of components c and the number of phases P plus two; i.e., $l = c - P + 2$. Thus such a monophasic two-component system has three degrees of freedom, that is, pressure, temperature, and moisture content (vapor pressure e, specific humidity q, or any other water vapor concentration parameter). Relative humidity in a moist atmosphere depends on temperature and moisture content (three degrees of freedom of the system).

If two phases of water, for example, liquid and vapor, are present at equilibrium, the atmosphere becomes saturated and has only two degrees of freedom. Thus the moisture quantity (e.g., the saturation vapor pressure e_s) at a given level becomes only a function of temperature, as confirmed by the Clausius–Clapeyron equation.

Because specific humidity and water vapor pressure can be regarded as independent parameters for the moist atmosphere, the climatologies of these quantities have an intrinsic meaning that the climatology of relative humidity lacks. Furthermore, specific humidity is more directly related to the radiative forcing. These considerations constitute a strong reason to take these independent parameters to define the climatology of water vapor in the atmosphere, as has been the usual approach (e.g., Peixoto and Oort 1983). On the other hand, the dependence of relative humidity on both the water vapor content and temperature makes relative humidity an attractive, dynamic parameter. The relative humidity values can be related to dynamical processes (such as advection, convection, and subsidence) that bring about changes in temperature or to other forms of diabatic heating (absorption of radiation, the release of latent heat, etc.). Also relative humidity can be regarded as an indicator of the possibility of phase changes in the atmosphere (cloud formation, precipitation, etc.). These facts explain the frequent use of relative humidity by modelers as a basic moisture parameter in their studies.

As we will see, the results of model simulations show that the atmosphere appears to maintain a somewhat uniform distribution of relative humidity over a wide range of atmospheric temperatures. Thus, an increase in temperature generally would lead to an increase of the amount of water vapor in the atmosphere and an increased absorption of thermal radiation (the "greenhouse effect"). This, in turn, would give rise to further increases in temperature of the atmosphere. In this connection, we note that the temporal and spatial relationships between tropical temperature and humidity have been studied extensively from radiosonde observations by Sun and Oort (1995) and have been compared with results from general circulation model (GCM) runs by Sun and Held (1996). These last authors find a remarkable degree of consistency between temperature and specific humidity variations, pointing to an almost constant relative humidity, in the model runs. However, in the observations the correlations between temperature and specific humidity were found to be much weaker (see also Gaffen et al. 1992). These differences between model and observations are somewhat surprising since the humidity in most GCMs is treated as an independent variable. We note that in the early one-dimensional model simulations of, for example, Manabe and Wetherald (1967), a constant relative humidity condition was imposed and was found to lead to fairly realistic climate simulations. The condition of an almost constant relative humidity has also been found in other GCM simulations of the water vapor feedback in greenhouse warming by, for example, Manabe and Wetherald (1975), Rind et al. (1991), and Mitchell and Ingram (1992), although they show some weak decreases in the tropospheric relative humidity during their GCM climate warming experiments. Emanuel (1994) argues, on the other hand, that the present convective parameterization schemes generally do not take into account the important cloud microphysical processes in an accurate way, sufficient for adequate climate simulations. Thus, in summary, we may say that there is a clear need for more definitive observational studies of the relative humidity climatology and its variability in the atmosphere.

Some thought must be given to the precision required in the observations. Besides the random errors, we must be aware of the instrumental difficulties involved in the measurements of humidity. The sensitivity and response time of the humidity sensor depends

on the type of instrument used. The response time always increases with lower values of relative humidity because the number of water vapor molecules decreases with height, and thus with lower temperatures. For the study of climate change and trends, the histories of the past observations, the computational methods, and the evaluation practices must be carefully documented (Gaffen 1993). However, for climatological studies based on time averages, the requirements are not as stringent. In the present study we are dealing with a broad sample in time and space, so that the results will depict only the main characteristic features of the relative humidity fields.

2. Theoretical framework

To help the discussion of our results, it is useful to show the dependence of the relative humidity on temperature and other moisture parameters. Furthermore, these expressions will facilitate the interpretation of the data and help to quantify some relations that otherwise would remain qualitative and less clear (see also Iribarne and Godson 1973).

The relative humidity U at a given temperature T is given by the ratio of the actual water vapor pressure e to the saturation vapor pressure e_s at the same pressure p and air temperature T. For all practical purposes, it can be given also by the ratio of specific humidity q and saturation specific humidity q_s

$$U = \frac{e}{e_s} \approx \frac{q}{q_s}. \tag{1}$$

As we know, the specific humidity q is related to the pressure p and water vapor pressure e by the expression

$$q = \epsilon \frac{e}{p + (1 - \epsilon)e}, \tag{2}$$

where $\epsilon = R_d/R_v$ ($\approx$0.622) and R_d and R_v are the gas constants for dry air and water vapor, respectively. It can be simplified to

$$q \approx \epsilon \frac{e}{p}. \tag{3}$$

The saturation pressure of water vapor e_s is an exponential function of temperature only, given by the Clausius–Clapeyron equation [Peixoto and Oort 1992, Eq. (3.65b)]

$$\frac{de_s}{dT} = \frac{Le_s}{R_v T^2} = \epsilon \frac{Le_s}{R_d T^2}, \tag{4}$$

where L = latent heat of phase transition that we will assume to be constant.

The temperature at which saturation is reached is called the dewpoint temperature T_d so that for this temperature the actual water vapor pressure becomes the saturated value ($e = e_s$). Thus, expression (4) reduces to

$$\frac{de}{dT_d} = \frac{Le}{R_v T_d^2}. \tag{5}$$

This relation shows that T_d and e are humidity parameters that give equivalent information.

If we integrate (4) between T_d and T, we obtain

$$e_s = e \exp\left[\frac{L}{R_v}\left(\frac{1}{T_d} - \frac{1}{T}\right)\right], \tag{6}$$

noting that for $T = T_d$, e is the saturation vapor pressure. Eqs. (1), (3), (4), and (5) form a closed system of four variables, for example, q, e, U, and T_d, or for q, U, T, and T_d, etc.

We will focus our discussion on the relative humidity parameter U and try to assess how it varies with specific humidity and temperature for an isobaric level (p = const). By differentiation of expression (1) we get

$$\frac{dU}{U} = \frac{de}{e} - \frac{de_s}{e_s} = \frac{dq}{q} - \frac{dq_s}{q_s}, \tag{7}$$

and from (3)

$$\frac{dq_s}{q_s} = \frac{de_s}{e_s} - \frac{dp}{p}. \tag{8}$$

For a given isobaric level (p = const)

$$\frac{dq_s}{q_s} = \frac{de_s}{e_s}, \tag{9}$$

and from (4)

$$\frac{de_s}{e_s} = \left(\frac{L}{R_v T}\right)\frac{dT}{T}. \tag{10}$$

Finally, inserting this expression (10) into (7), we obtain

$$\frac{dU}{U} = \frac{dq}{q} - \left(\frac{L}{R_v T}\right)\frac{dT}{T}. \tag{11}$$

This is the desired expression that relates the relative fluctuations of the relative humidity U to the relative fluctuations of specific humidity and temperature. As we see, the contributions of the relative fluctuations of q and T to the fluctuations in U are of opposite sign.

The variation dT may be due to diabatic heating and to adiabatic effects (cooling with adiabatic expansion and warming with adiabatic compression). Therefore, with rising adiabatic motion the cooling of the air lowers the value of the saturation water vapor pressure and increases the relative humidity. On the other hand, with subsidence the saturation water vapor pressure will increase leading to a decrease in relative humidity.

To get an order of magnitude estimate of the influence of temperature on U, we computed the coefficient

(L/R_vT) for various temperatures (T = 260 K–285 K) using a constant L_v = 2500 J g^{-1} and a constant R_v = 466.5 J kg^{-1} K^{-1}. The final values for L/R_vT range between 20.8 and 18.9. Thus, for average conditions in the lower atmosphere, this coefficient is about 20, and (11) can be written as

$$\frac{\Delta U}{U} = \frac{\Delta q}{q} - 20\frac{\Delta T}{T}. \tag{12}$$

For a constant relative humidity, the relative fluctuations of q are 20 times those of T. In other words, for a 1% change in temperature (~3 K) the specific humidity will change by 20%. Analogously, for a constant specific humidity, the relative variations of U are also 20 times the relative variations of T.

To show how the relative humidity U is related to the dewpoint temperature T_d and to the air temperature T, we can start with the Clausius–Clapeyron equation (6). Noting that $U \equiv e/e_s$, we have then

$$U^{-1} = \exp\left[\frac{L}{R_v}\left(\frac{1}{T_d} - \frac{1}{T}\right)\right]$$

or

$$-\ln U = \frac{L}{R_v}\left(\frac{1}{T_d} - \frac{1}{T}\right). \tag{13}$$

After differentiating (13), we obtain

$$\frac{dU}{U} = \frac{L}{R_v}\left[\frac{dT_d}{T_d^2} - \frac{dT}{T^2}\right]. \tag{14}$$

Equation (14) shows the relation between the variations of U and the variations of T and T_d; the two contributions are of opposite sign. Thus, when T_d increases, U increases also ($\Delta T_d > 0 \rightarrow \Delta U > 0$), and when T increases, U decreases ($\Delta T > 0 \rightarrow \Delta U < 0$).

Using the same approach as in establishing (12), we obtain for the relative variations of U the following approximate expression:

$$\frac{\Delta U}{U} \approx 20\left(\frac{\Delta T_d}{T_d} - \frac{\Delta T}{T}\right), \tag{15}$$

which shows again the importance of the variations of T and T_d for the relative humidity. A relative variation of 1% in T or T_d leads to a 20% variation in relative humidity, which shows how sensitive the relative humidity is to small variations in T or T_d. However, we must keep in mind that variations in T and T_d have opposite effects on the relative humidity.

During the course of a day, assuming that p is constant and that q does not change, we find from (11)

$$\frac{dU}{U} = -\left(\frac{L}{R_vT}\right)\frac{dT}{T}. \tag{16}$$

Under these conditions, the variations of U and T during the course of a day are of opposite sign or, in other words, they are 12 hours out of phase. Thus, the maximum of U will usually occur in the early morning hours (at sunrise) and the minimum in the early afternoon. Of course, in the case of stations where sea breeze occurs during the afternoon, the variation of U during the day may be distorted and a maximum could occur in the early afternoon.

Let us consider now the variation of relative humidity during an adiabatic ascent assuming that the water vapor content, as given by the molar fraction N_v, remains constant. It is easy to show that under these conditions the water vapor pressure e follows a Poisson-like equation

$$Te^{-\kappa} = \text{const}, \tag{17}$$

where $\kappa = R_d/c_p$ is the Poisson constant. After some mathematical manipulations and using the Clausius–Clapeyron equation, expression (7) can be written in the form

$$\frac{dU}{dT} = \frac{U}{T}\frac{c_pT - \epsilon L}{R_dT}, \tag{18}$$

which gives the rate of change of the relative humidity with temperature in an adiabatic expansion. In the atmosphere the expression ($c_pT - \epsilon L$) is in general negative so that $dU/dT < 0$. Because the temperature decreases with height, the relative humidity increases and saturation can then be reached. Thus, for average conditions in the lower troposphere during an adiabatic ascent the relative variation of the relative humidity is given approximately by

$$\frac{\Delta U}{U} \approx -14\frac{\Delta T}{T}. \tag{19}$$

In other words, for a constant moisture content the relative fluctuations of U are fourteen times those of T. Note that under constant pressure conditions [see expression (12)] the relative variations are 20 times instead of 14 times in the present case of adiabatic expansion.

The expressions (12) and (18) raise the important issue of using a purely thermodynamical analysis to explain the large-scale climatology of relative humidity. In fact, for the relative humidity variations, one has to consider how the dynamics of the circulation affect the changes in temperature and specific humidity, as well as the phase transitions.

3. Data and analysis techniques

a. General comments

The primary observing system for the atmosphere is the radiosonde network. The observations are taken mainly for operational purposes, and the quality of the soundings is not always sufficiently high. Nevertheless, the radiosonde system is still one of the most accurate observing systems: temperatures are measured within

±0.5°C, pressures within ±1 hPa (= 1 mb), and relative humidities within ±5% or with even higher accuracy (Elliott and Gaffen 1991). Errors become larger at higher levels where the low density leads to slower response times and the shielding of solar and thermal radiation becomes more difficult.

Besides the inherent random errors, there have been changes in instruments and in data reduction procedures, errors in coding and reporting practices, etc. The issue can be raised how representative point measurements are, in general, for the larger surrounding volume of the atmosphere. This problem is still more severe when we consider the humidity measurements. The humidity field is patchy and changes on short time and space scales, so that there is some question whether a single ascent is sufficiently representative for a broad region (in both time and space).

Of course, besides these shortcomings of the individual soundings, we must be aware of the errors in measuring the global water vapor field. Because the radiosonde network is highly biased toward the Northern Hemisphere land areas (see Fig. 1), the fields over the oceans and in the Tropics are poorly observed. The most remarkable gaps are in the Southern Hemisphere oceans and in the eastern equatorial Pacific.

b. Sources of data

In the present study we used twice-daily radiosonde data from the global network for a period of 15 years, from May 1973 through April 1988. To discard obviously erroneous humidity values, daily station reports of specific humidity that deviated more than four standard deviations from the long-term seasonal mean at the station location were discarded and not used in the further analyses of specific and relative humidity (see Oort 1983; updated). The choice of four standard deviation cutoff was reached after looking at what data were discarded and represents a subjective judgement. To investigate the quality of the monthly mean data, a subset of a few hundred consistently reporting stations (i.e., stations with 10 or more observations of humidity during a month throughout the 15-yr period) from the global network was selected both for 0000 and 1200 UTC up to 300 mb. The time series of the monthly means for each station were plotted and carefully screened by eye to develop some sense of the degree of homogeneity in the data. The humidity data were especially scrutinized to find jumps in the time series and unrepresentative values (Oort 1983). Although some first estimates could be made of the quality of the data for later applications, such as time series analyses and trend analyses (Oort 1993, 1994), all monthly station values from the period May 1973–April 1988 were used in the present study.

It is evident from Table 1 showing the number of good stations reporting at the various levels that the analyses must be most reliable at the mid tropospheric levels 850, 700, and 500 mb. Below 850 mb the number of reports drops off because of the interference of topography and the fact that often stations report only at the standard pressure levels of 1000 and 850 mb.

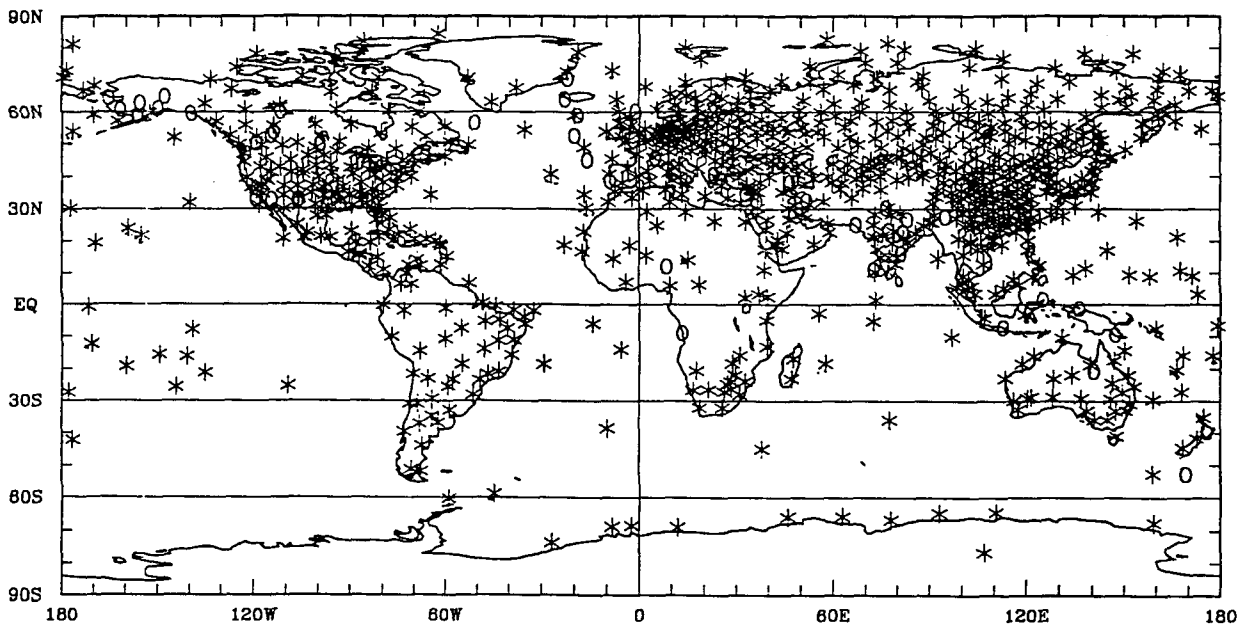

FIG. 1. Global distribution of "good" radiosonde stations (i.e., $N_{day} \geq 10$ mo^{-1}) reporting humidity during the May 1973–April 1988 period. An asterisk ("*") indicates a station reporting adequately both at the 500- and 300-mb levels ($12 \leq N_{mo}^{500}, N_{mo}^{300} \leq 180$), whereas a zero ("0") indicates a station with insufficient reports at the 300-mb level ($12 \leq N_{mo}^{500} \leq 180$, but $N_{mo}^{300} < 12$) (see also Table 1).

TABLE 1. Number of radiosonde stations containing at least ten observations per month as a function of pressure level and the number of reporting months during the period May 1973–April 1988 (maximum of 180 months). Note that *all* available stations were used in the analysis for a particular month. In other words, even when a station only reported for one month and not for any of the other 179 months, it was used for that particular month.

Range of number of months	Pressure (mb)							
	1000	950	900	850	700	500	400	300
120–180	413	433	437	699	718	712	656	473
60–119	118	120	121	127	140	148	173	241
12–59	124	212	256	138	142	145	163	206
1–11	89	113	133	92	95	94	94	114
1–180	744	878	947	1056	1095	1099	1086	1034

Thus in case the 1000 mb and surface reports are missing, there is no information below 850 mb, except for those stations that report at 950 and 900 mb (such as the North American stations) or at other significant levels. Above 400 mb, the humidity measurements become less reliable especially under very cold, dry conditions, for example, in the polar upper troposphere (see section 3c).

To present maps of the surface relative humidity over the oceans that are more representative than the (more problematic) 1000-mb maps derived from the radiosonde network, we have used our analyses of the Comprehensive Ocean–Atmosphere Data Set (COADS; Woodruff et al. 1987) for the same 15-yr period May 1973–April 1988. Monthly analyses were made using the Levitus (1982) analysis scheme based on the surface humidity reports from ships. Similar quality checks (see, e.g., Pan and Oort 1983) were performed as were used with the radiosonde data. Of course, the COADS reports are taken at ship deck level, ideally at about 10-m height, whereas the height of the 1000-mb radiosonde reports is generally on the order of 100 m, although it may vary strongly in space and time. Thus, overall, we would expect somewhat higher relative humidities in the COADS reports because of the closer proximity to the source of the water vapor, the ocean surface, in spite of the temperatures being a little higher.

Other data sources used to validate our relative humidity analyses are satellite observations of upper-tropospheric relative humidity by the Stratospheric Aerosol and Gas Experiment (SAGE) (section 5a), independent operational analyses produced at the European Centre for Medium-Range Weather Forecasts (ECMWF, section 5b), and cloud observations made from the surface (section 5c). The specific characteristics of each of these datasets will be discussed in the relevant sections of this paper.

c. *Limitations of the data*

Basically the radiosondes measure the pressure p (directly or indirectly), the temperature T, and the relative humidity U. Most of the radiosondes use aneroid capsules, baroswitches, or, in many cases, radar observations to evaluate pressure. The temperature sensors most widely used are bimetal strips and thermistors. In some cases tungsten-rod resistance sensors are used. To avoid the influence of solar radiation, the bimetallic sensors are shielded and the thermistors are covered by a white reflective paint.

The humidity sensors can be based on organic material, such as goldbeaters' skin and human hair, or on hygrometers using humidity-resistance relationships, such as lithium chloride, carbon hygristors, capacitive sensors (Vaisala radiosondes), etc.

Humidity measurements in the free atmosphere are probably the least satisfactory compared to pressure and temperature measurements at the present time due to the high variability in humidity and instrumental difficulties. The sensitivity of the sensor varies with the type of sensor used, and the lag coefficient usually increases at low temperatures decreasing the fidelity of the data. In some cases the dependence of the humidity sensor on temperature is so strong that at lower temperatures the reaction of the sensor ceases. In some resistance-based instruments (e.g., U.S. radiosondes) so-called motorboating may occur when $U < 20\%$ and $T < -40°C$ (a common situation in the upper troposphere). At this low level of intensity, the electric relative humidity circuit can be interrupted because the relative humidity element does not react, and the sound of the radiosonde receiver resembles the sound of a motor boat instead of being continuous (see Nash and Schmidlin 1987; WMO 1983).

The observed quantity for water vapor is relative humidity U. This quantity and the measured temperature T are converted into the dewpoint depression, $T - T_d$, for transmission. The conversion depends upon the type of algorithm used that sometimes varies from country to country (WMO 1983; Nash and Schmidlin 1987; Elliott and Gaffen 1991). This by itself is already a source of inhomogeneity. Furthermore, the constraints imposed on the process of coding for transmission can bring some additional uncertainties since for low values of $T - T_d$ the values are rounded to tenths of a degree.

d. Computation and analysis of relative humidity

For our study we recovered the relative humidity data at various pressure levels using the twice-daily reported values T and T_d and the expression (1):

$$U = \frac{e}{e_s} \approx \frac{q}{q_s}.$$

The saturation vapor pressure e_s, which is a function only of temperature, was computed using the empirical exponential formula of Tetens (1930):

$$e_s = 6.11 \times 10 \exp\left(\frac{at}{t+b}\right), \qquad (20)$$

where the constants a and b over water are $a = 7.5$ and $b = 273.3$, and t is in degrees Celsius. This is a version of the well-known Magnus formula (Saucier 1955). Using T_d instead of T we obtained the actual vapor pressure e. The long-term mean annual and seasonal mean values of relative humidity were then evaluated from

$$\bar{U} = \overline{\left(\frac{e}{e_s}\right)}, \qquad (21)$$

where the overbar indicates the time average $\bar{(\ )} = \int_0^\tau (\ )dt/\tau$. All daily station data were screened and erroneous values of humidity were discarded at each level using a $\bar{U} \pm 3.5\sigma(U)$ discard criterion (see earlier discussion in section 3b).

This last expression (21) is obviously different from

$$\bar{U}^\dagger = \frac{\bar{e}}{\bar{e}_s} \approx \frac{\bar{q}}{\bar{q}_s} \qquad (22)$$

that has sometimes been used. Indeed, expression (21) can be written as

$$\bar{U} = \overline{\left(\frac{\bar{q} + q'}{\bar{q}_s + q'_s}\right)} = \bar{U}^\dagger \overline{(1 + q'/\bar{q})(1 + q'_s/\bar{q}_s)^{-1}}.$$

After a series expansion, we find

$$\bar{U} \approx \bar{U}^\dagger(1 + \overline{q'^2_s}/\bar{q}^2_s - \overline{q'q'_s}/\bar{q}\bar{q}_s), \qquad (23)$$

where the prime indicates a departure from the time mean value. From (23) we see that the difference $\bar{U} - \bar{U}^\dagger$ depends on the variance of q_s and the covariance of q and q_s, or since q_s is only a function of T, the difference also depends on the variance of temperature and the covariance of q and T. The two correction terms on the right-hand side of (23) are of opposite sign so there may be some compensation. However, noting that the denominator of the first term is larger than the denominator of the second term ($\bar{q}^2_s > \bar{q}\,\bar{q}_s$), we see that the difference $\bar{U} - \bar{U}^\dagger$ can be either positive or negative. We will use these considerations further in the final section of this paper.

e. Objective analysis techniques

The twice-daily radiosonde soundings were composited into monthly station statistics, and only those stations with more than 10 validated reports at a particular level were used to generate maps. To interpolate the mean monthly values from the rawinsonde network (see Fig. 1) to a regular 2.5° latitude by 5° longitude global grid, the "ANAL68" objective analysis procedure was used. In this procedure, a conditional relaxation analysis method (Harris et al. 1966) was used to fit a smooth surface through the radiosonde values. Several analysis cycles were then performed with decreasing degrees of smoothing of the anomalies from the first guess field (see, e.g., Oort 1983; Peixoto and Oort 1992).

The individual monthly analyses were next composited into 15-yr mean seasonal and annual analyses using all available data from the period May 1973–April 1988. The main quantities discussed in this paper are the mean relative humidity $\bar{U}$ and the temporal standard deviation of relative humidity $(\overline{U'^2})^{1/2}$. Here the overbar indicates the 45-mo seasonal or 180-mo annual mean value, and the prime denotes a departure from the corresponding mean value. Thus, all variations with periods less than 3 mo as well as interannual variations are included in the seasonal variances $\overline{U'^2}$, whereas all variations less than 15 yr are included in the annual variance $\overline{U'^2}$. In addition to the relative humidity, certain measures of the temperature T and specific humidity q will also be presented when necessary. Besides horizontal maps, we will show various zonal mean cross sections and vertical profiles of the hemispheric and global mean values. The zonal mean will be indicated by square brackets and the departure from a zonal mean by an asterisk so that for relative humidity

$$U = [U] + U^*.$$

4. Analysis of results

a. Correlations between different global fields

To help the discussions of the global fields of relative humidity, we show in Table 2 some spatial correlation coefficients between the fields of mean relative humidity and those of mean temperature, specific humidity, and vertical (pressure) velocity computed for the Tropics (30°S–30°N) and midlatitudes (30°–60°S, 30°–60°N). We have used a "resistant" (Spearman rank order) technique to estimate the correlation coefficients since it reduces the influence of outliers and is more appropriate than the traditional (Pearson) correlation coefficient when the data are not normally distributed (Lanzante 1996). To test the null hypothesis that the population value of the correlation coefficient $\rho(x, y)$ equals zero, we used the so-called Fisher's Z transformation (Spiegel 1961; Oort and Yienger 1996) for $r(x, y)$ and determined cutoff values $r_0(x, y)$ as a function

TABLE 2. Spatial "resistant" correlation coefficients (see text) between the 15-yr mean fields of relative humidity ($\bar{U}$) and those of temperature ($\bar{T}$), specific humidity ($\bar{q}$), and vertical (pressure) velocity ($\bar{\omega}$) for the Tropics (30°S–30°N) and midlatitudes (30°–60°S, 30°–60°N). Values that are computed to be statistically significant at the 95% confidence level assuming a "reasonable" number of degrees of freedom (N_{df}; see text) are printed in bold.*

	$r(\bar{T}, \bar{U})$			$r(\bar{q}, \bar{U})$			$r(\bar{\omega}, \bar{U})$		
	$N_{df} = 20$			20			30		
Tropics	DJF	JJA	ANN	DJF	JJA	ANN	DJF	JJA	ANN
300 mb	0.34	**0.55**	**0.44**	**0.86**	**0.85**	**0.80**	−0.35	**−0.52**	−0.33
500 mb	**0.52**	**0.44**	**0.53**	**0.94**	**0.93**	**0.91**	**−0.44**	**−0.60**	**−0.46**
700 mb	0.29	**0.45**	0.33	**0.92**	**0.94**	**0.93**	**−0.47**	**−0.56**	**−0.44**
850 mb	0.02	0.03	−0.15	**0.71**	**0.76**	**0.76**	−0.17	−0.20	−0.07
900 mb	0.19	0.28	0.11	**0.70**	**0.75**	**0.76**	−0.18	−0.21	−0.10
950 mb	0.25	0.38	0.19	**0.68**	**0.73**	**0.72**	−0.19	−0.24	−0.13
1000 mb	0.16	0.24	0.08	**0.52**	**0.54**	**0.51**	−0.16	−0.24	−0.12
	$r(\bar{T}, \bar{U})$			$r(\bar{q}, \bar{U})$			$r(\bar{\omega}, \bar{U})$		
	$N_{df} = 15$			15			25		
Midlatitudes	DJF	JJA	ANN	DJF	JJA	ANN	DJF	JJA	ANN
300 mb	**−0.73**	**−0.52**	**−0.80**	**−0.50**	−0.09	−0.35	−0.16	−0.26	−0.19
500 mb	**−0.79**	−0.46	**−0.79**	**−0.62**	−0.09	−0.40	−0.10	−0.21	−0.11
700 mb	**−0.74**	−0.31	**−0.80**	**−0.56**	0.10	−0.41	−0.23	−0.25	−0.27
850 mb	−0.40	−0.22	−0.40	−0.16	0.09	−0.10	−0.37	−0.20	−0.34
900 mb	−0.16	−0.11	−0.16	−0.01	0.10	0.04	−0.28	−0.14	−0.24
950 mb	−0.06	−0.05	0.00	0.07	0.13	0.16	−0.19	−0.06	−0.15
1000 mb	−0.06	−0.44	−0.20	0.06	−0.26	−0.11	−0.09	−0.21	−0.16

* The cutoff values $r_0(x, y)$ as a function of the number of degrees of freedom are given below:

N_{df}	5	10	15	20	25	30	50	100
r_0	0.88	0.63	0.51	0.44	0.40	0.36	0.28	0.22.

of the number of degrees of freedom (N_{df}). The results are given in a footnote at the bottom of Table 2. We estimated N_{df} by eye by carefully studying the spatial structure of the global fields of $\bar{U}$, $\bar{T}$, $\bar{q}$, and $\bar{\omega}$ for the different seasons and by looking at scatterplots like those shown in Fig. 2. In general, there is more small-scale structure in the tropical relative humidity (see Figs. 3b and 3c) and, especially, the vertical velocity fields (not shown) compared to the structure in the temperature and specific humidity fields. While the determination of N_{df} is subjective, it is not clear how to make a more quantitative estimate since the fields of interest are climatological means. The chosen values for N_{df} are shown in Table 2, and the significant r-values, according to our criterion, are printed as bold numbers. Of course, the reader can choose his/her own criterion of significance using the cutoff values in the footnote.

The results presented in Table 2 show striking differences between the Tropics and midlatitudes. In the Tropics one finds that the relative humidity $\bar{U}$ is primarily determined by the specific humidity $\bar{q}$ (see Fig. 2a) and that temperature variations play only a minor role. High values of relative humidity tend to go together with high specific humidity, and vice versa. During all seasons the values are highly significant $r(\bar{q}, \bar{U}) \geq 0.7$–$0.9$. The correlations with the vertical velocity field $\bar{\omega}$ (only shown for $\bar{U}$) show that in the Tropics convective processes clearly dominate with the rising ($\bar{\omega} < 0$) of relatively warm, humid (both specific and relative) air, and the sinking of relatively cold, dry air. In other words: $r(\bar{\omega}, \bar{T}) < 0$, $r(\bar{\omega}, \bar{q}) < 0$, and $r(\bar{\omega}, \bar{U}) < 0$ (see also Fig. 2c).

In the midlatitudes, Table 2 shows that the relative humidity is primarily determined by the temperature variations (see also Fig. 2b), showing a strong negative correlation above 850 mb probably associated with advective processes. Cold air originating from the north will tend to maintain its moisture and thus increase its relative humidity, while warm air from the south will have lost some of its moisture due to condensation, leading to an overall $r(\bar{T}, \bar{U}) < 0$ and $r(\bar{q}, \bar{U}) < 0$ in midlatitudes. It is interesting to note that these correlations are weaker in summer when tropical influences (of the opposite sign) penetrate into midlatitudes. The correlations with the vertical motion field are not significant.

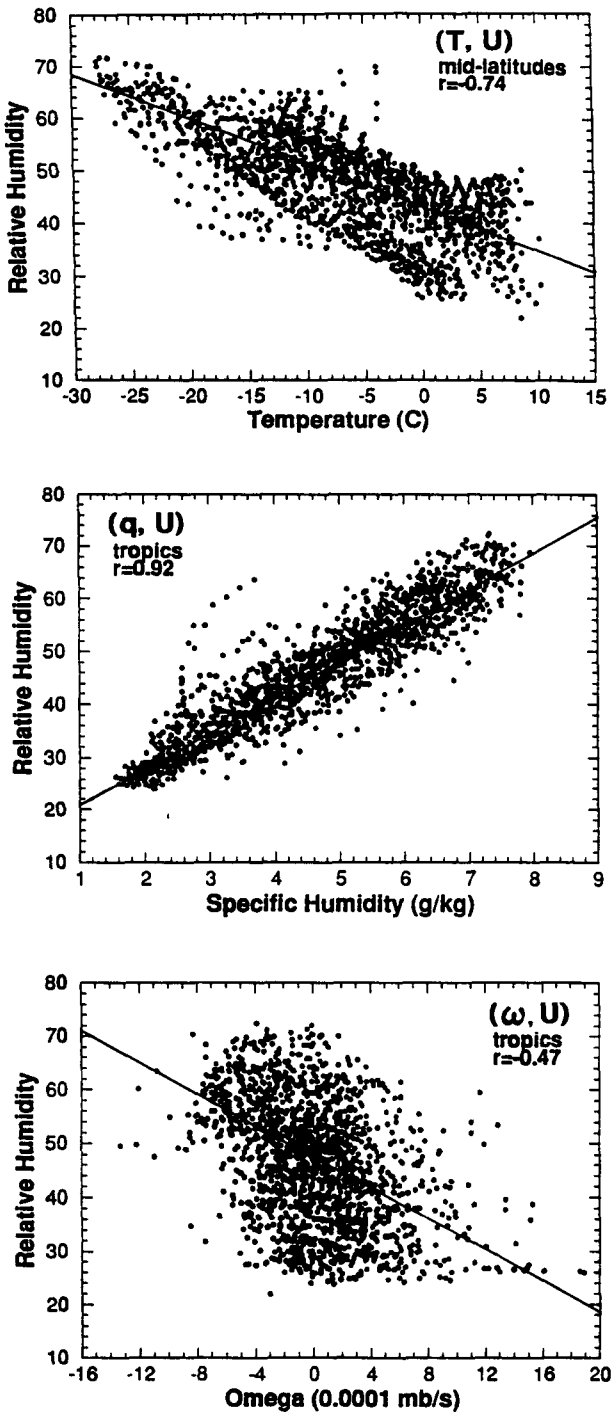

FIG. 2. Scatterplots of the grid point values (2.5° latitude, 5° longitude) for the 15-yr mean December–February conditions at 700 mb for $\bar{U}$ versus $\bar{T}$ in midlatitudes (top), $\bar{U}$ versus $\bar{q}$ in the Tropics (middle), and $\bar{U}$ versus $\bar{\omega}$ in the Tropics (bottom). The resistant estimate of the regression slope using the median of pairwise slopes (Lanzante 1996) is shown as a solid line in each diagram. The units for relative humidity are percent, for temperature degrees Celsius, specific humidity grams per kilogram, and vertical velocity 10^{-4} mb s^{-1}.

b. Global distributions at various levels

The time-mean distributions of relative humidity at the ocean surface and at the 850- and 500-mb levels are presented for annual and extreme seasonal conditions in Fig. 3. The areas where the pressure level dips below the topography are blacked out. Only values above the topography are included in the further calculations. Since the 1000-mb analyses based on the radiosonde network are relatively poor (see Table 1 and earlier discussion), we present in Fig. 3a the surface analyses over the oceans based on the COADS instead. The COADS fields show a much more detailed structure than the 1000-mb analyses (not shown), which is to be expected since more data points were available in the COADS.

The highest values of relative humidity occur in the equatorial zone where the mean water vapor content of the air and the temperature are high. In this zone, the tropical convective systems connected with the intertropical convergence zone (ITCZ) dominate the circulation with a strong vertical transport and diffusion of water vapor associated with the ascending branch of the Hadley cell (see expression 18 for adiabatic upward motion) leading to the high relative humidity. Away from the equatorial belt, the relative humidity decreases toward the subtropical regions because deep convection is suppressed by mean downward motion of the air in the subtropical high pressure belts. Of course, in the subtropics the cloudiness and precipitation are also a minimum due to the high subsidence and divergence at low levels, in spite of the high incidence of solar radiation that leads to strong evaporation in the subtropical belts. By and large, the distributions are not zonally uniform. They show centers of various intensities at all latitudes.

In mid to high latitudes relative humidity, precipitation, and cloudiness increase again due to the baroclinic disturbances associated with the polar front. This increase of relative humidity with latitude is due to moisture advection from the subtropics and the decrease in temperature [see Eq. (12) and Fig. 2b]. Poleward of 60° latitude, the relative humidity remains constant or increases slightly. As mentioned earlier in section 2, it is clear that an explanation of the relative humidity climatology has to be based on both thermodynamical and dynamical arguments.

The seasonal migration of the belts of maximum relative humidity over the equatorial region is associated with the displacement of the ITCZ and the seasonal interhemispheric shifts of the continental convective areas over Asia, Australia, and the Americas. The seasonal variations are more pronounced in the Northern Hemisphere where the ITCZ is connected with a deeper convection reinforced by the stronger release of latent heat in the upward branch of the Hadley cell. During northern summer June–August (JJA), the ITCZ penetrates farther into the Northern Hemisphere, bringing

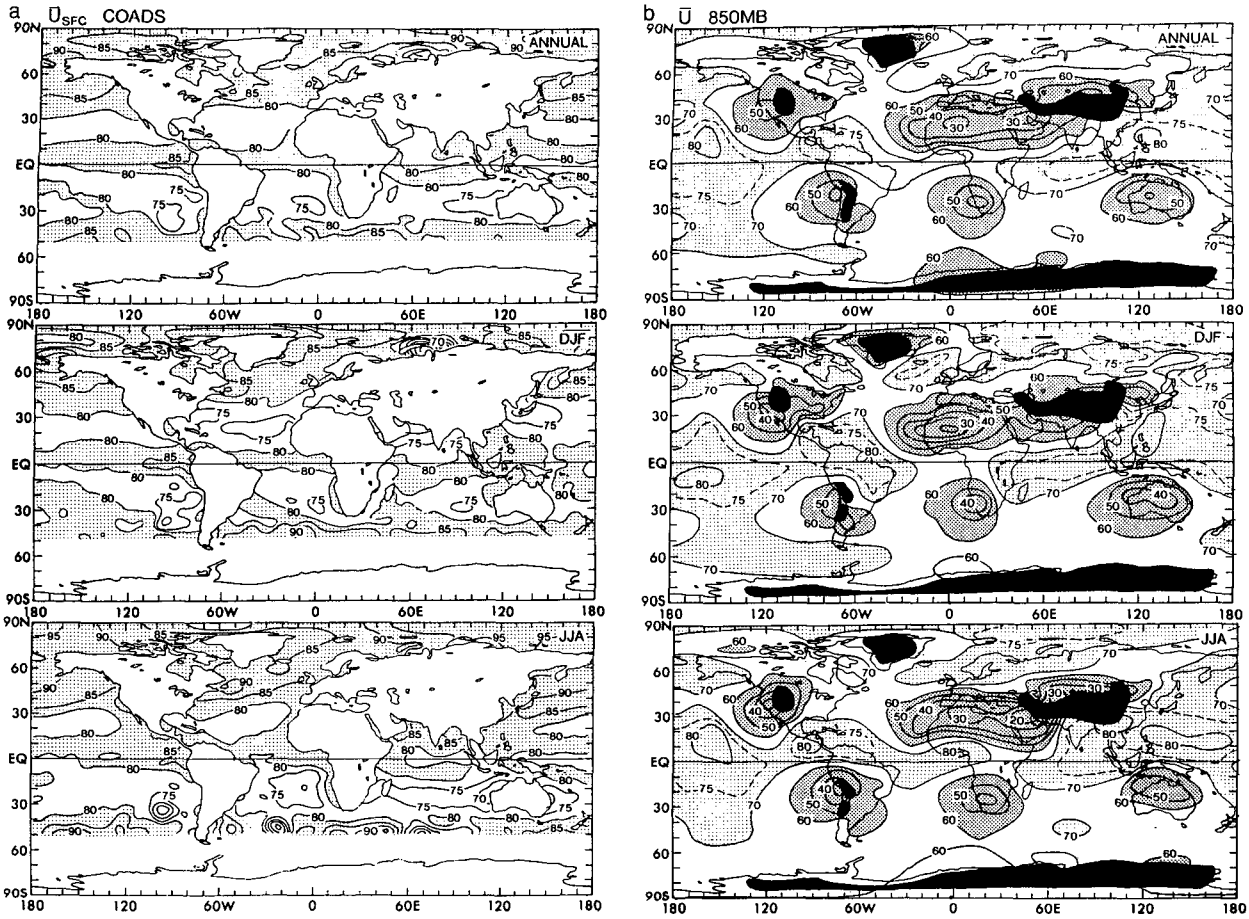

FIG. 3. (a) Global distributions of the mean relative humidity (%) for the annual and extreme seasonal conditions at the ocean surface averaged over the 1973–86 period based on COADS. Areas with $\bar{U} > 80\%$ are shaded. (b) Global distributions of the mean relative humidity (%) for the annual and extreme seasonal conditions at the 850-mb level averaged over the 1973–86 period. Heavy shading indicates $\bar{U} < 60\%$, and light shading areas with $U > 70\%$. Areas below the mountains are blacked out.

moist air masses to the tropical North Pacific, Central America, Equatorial Africa, etc., resulting in high values of relative humidity. The largest values of relative humidity occur over the Amazon region, Southeast Asia, Malaysia, and the Indonesian Archipelago at all levels. These are regions of strong convergence (high vertical motion) and shallow, warm waters, providing a large supply of water vapor. On a regional scale, the largest variability of relative humidity is by far found in the Amazon and Asian monsoon regions that we will discuss later. During the northern winter, December–February (DJF), the equatorial maximum in relative humidity lies somewhat south of the equator.

In the belt between about 30°N and 30°S the relative humidity tends to be higher during the summer season of each hemisphere. In northern winter, the subtropical minima are displaced to the south so that the dry zone in the Northern Hemisphere is closer to the equator, whereas in the Southern Hemisphere it is farther away from the equator. On the other hand, during the June–August season the opposite takes place, that is, the dry zones are displaced toward the north. The descending branch of the Hadley circulation with persistent subsidence over the subtropical high pressure belt between about 12° and 30°N, where most of the deserts are found, is responsible for the low values of relative humidity in that belt. Also, throughout the year subsidence tends to occur on the lee side of the great mountain ranges, favoring the formation of deserts and pronounced dryness, for example, the desert area of southwest America on the lee side of the Rocky Mountains, the Gobi Desert in Central Asia on the lee side of the Himalayas, and the deserts in Peru and Patagonia associated with the Andes Mountains. However, in the Southwest United States, there is a pronounced increase of relative humidity at all levels during June–August due to a summer monsoon flow from the Gulf of Mexico. The deserts in South America cannot be well resolved here because of the coarse spatial resolution of our analyses and

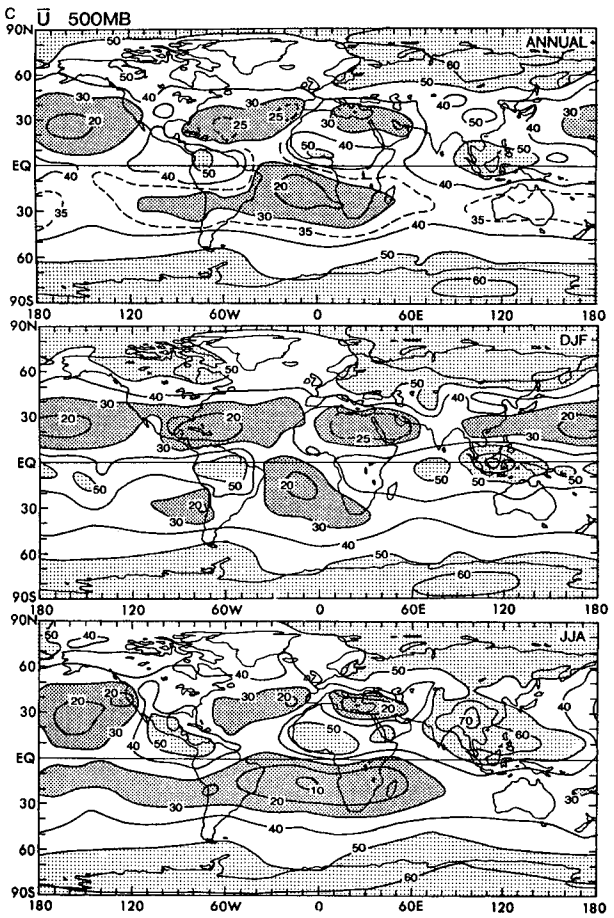

FIG. 3. (*Continued*) (c) Same as (b) except for 500 mb. Heavy shading indicates areas with $\bar{U} < 30\%$, and light shading areas with $\bar{U} > 50\%$.

the sparseness of the radiosonde network in the Southern Hemisphere.

The patterns discussed above can be explained by using again expressions (12) and (19). Although the specific humidity is usually larger in summer than in winter, the temperatures (and thus the saturation specific humidity) are so high that the relative humidity attains a minimum. This effect is more pronounced over the continents, where the influence of temperature on relative humidity is greater. However, we find a striking exception over North America, where higher humidities are found in summer. These high humidity values are due to the strong northward transport of water vapor from the Gulf of Mexico during that season (Starr et al. 1958). Rasmusson (1967) has shown that much of the inflow of moisture is associated with a low-level jet stream from the Gulf.

The existence of the Gulf of Mexico to the south (a large source of moisture) and of large mountain barriers to the west of the North American continent (guiding the flow northward) constitute a unique situation over the globe. These facts explain the exceptional high relative humidities observed over the North American continent during summer.

To summarize and better assess the vertical distribution of relative humidity, zonal-mean-averaged values are plotted as a function of latitude and pressure. The diagrams thus obtained are shown in Fig. 4. The general pattern of behavior of relative humidity is similar at mid- and low tropospheric levels. However, its magnitude decreases with altitude from values on the order of 70%–80% near the earth's surface to 30%–50% at the 300-mb level. The cross sections also show the importance of both the upward transport of moisture at the equator where a relative maximum in U is found (in the ascending branch of the Hadley cells) and the subsidence over the subtropical regions where the air is relatively dry with minima near 30° latitude. The relative humidity increases again poleward of these latitudes. The vertical trough and ridge lines (lines of minimum and maximum U) show a slight inclination toward the equator with height. The trough line in each hemisphere also moves toward the equator from summer to winter.

To get a measure of the fluctuations of relative humidity associated with the seasonal changes, we also computed the difference between the DJF and JJA cross sections of $[\bar{U}]$. The results are presented in the

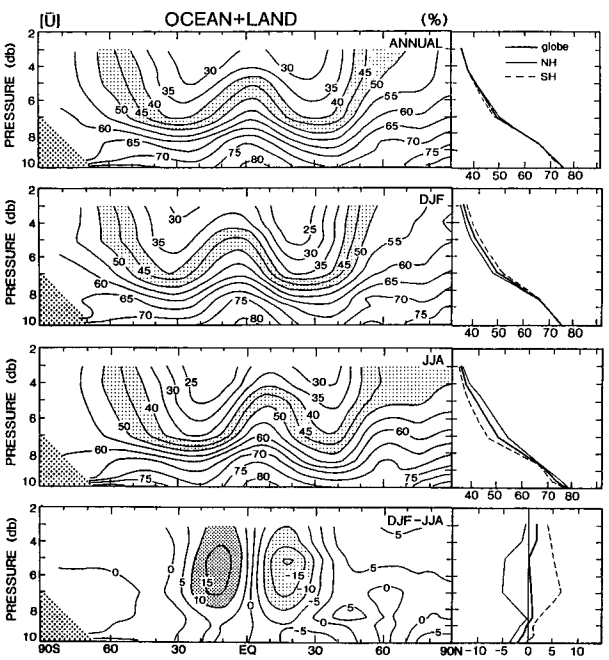

FIG. 4. Zonal mean cross sections of the relative humidity (%) for annual, DJF, and JJA mean conditions, and for the interseasonal variation, DJF–JJA. Vertical profiles of the hemispheric and global mean values are shown on the right. In the top three diagrams the areas with $40 < \bar{U} < 50\%$ are shaded. In the bottom diagram, areas where the differences are greater than 10% are shaded heavily and those where they are less than −10% are shaded lightly.

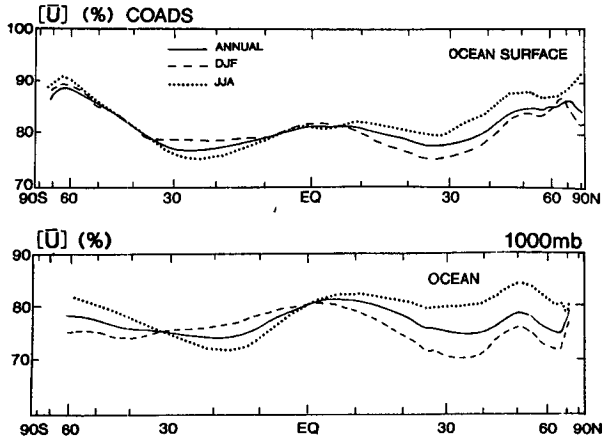

FIG. 5. Meridional profiles of the zonal mean relative humidity (%) over the ocean surface from the COADS (top), and at 1000 mb based on the radiosonde reports (bottom).

bottom diagram of Fig. 4. They show that the main fluctuations occur at low latitudes with maxima in the middle atmosphere near about 15°N and 15°S latitude with opposite sign in the two hemispheres. The maximum differences are on the order of 15%, which again shows that the constancy of relative humidity cannot be accepted in general. Moreover, we must take into account that these are differences in the zonal average and that locally the differences may be much greater. At mid- to high latitudes the differences are positive in the Northern Hemisphere and slightly negative in the Southern Hemisphere, showing that at these latitudes the relative humidity of the atmosphere tends to be larger during the winter season.

The vertical profiles on the right side of Fig. 4 synthesize the previous discussion, showing a decrease of relative humidity with height and seasonal variations of about 5%. The hemispheric profiles for DJF–JJA show very clearly the seasonal differences with a maximum in summer and a relatively flat extreme in the midtroposphere.

In Fig. 5 zonal-mean 1000-mb profiles of the relative humidity over the oceans (based on the sparse rawinsonde network) are compared with the corresponding COADS profiles. Both profiles show a maximum in the northern equatorial belt and minima in the subtropics, but they differ in the mid and high latitudes. The 1000-mb values are slightly lower than the surface values. These differences are related to the variations in the mean sea surface pressure with respect to 1000 mb and the decrease of moisture content away from the ocean surface. The mixing in the lower planetary boundary layer through turbulence and diffusion leads to a larger homogeneity shown in the lower seasonal variability of the surface profiles. Thus, the COADS data show a seasonal range in the Northern Hemisphere on the order of 5% and the 1000-mb rawinsonde values a range of about 10%. The 1000-mb profiles agree well with the profiles based on the maps published by Szava-Kovats as presented in Haurwitz and Austin (1944).

The saturation deficit $\bar{q}_s - \bar{q}\,[=\bar{q}_s(1-\bar{U})]$ was also evaluated and is presented in Fig. 6. Maxima are found in the mid- to lower troposphere at subtropical latitudes, being most intense over the Northern Hemisphere and in the summer season. They are slightly displaced equatorward compared to the axes of minimum relative humidity. This is due to the variations of relative humidity with temperature (through q_s) and specific humidity. The hemispheric and global mean profiles of $q_s - q$ on the right-hand side of Fig. 6 show very small vertical gradients below 700 mb and a rapid decrease above 700 mb.

c. *Land–sea contrast*

The maps in Fig. 3 show already that there is a considerable variability of relative humidity in latitude and longitude both at the lower and higher levels. However, there are more clear-cut differences when we compare the average fields over the oceans to those over the continents at the same latitude. Of course, there is also some variability within the oceanic and continental regions themselves.

Over the continents, we can distinguish several regions according to their different climates (the regions with monsoonal climates, desert climates, wet climates, tropical wet and tropical dry climates, etc.; see, e.g., Haurwitz and Austin 1944; Gaffen et al. 1992). We will not give a systematic discussion of our fields based on these climatic regions since it is beyond the scope of this paper.

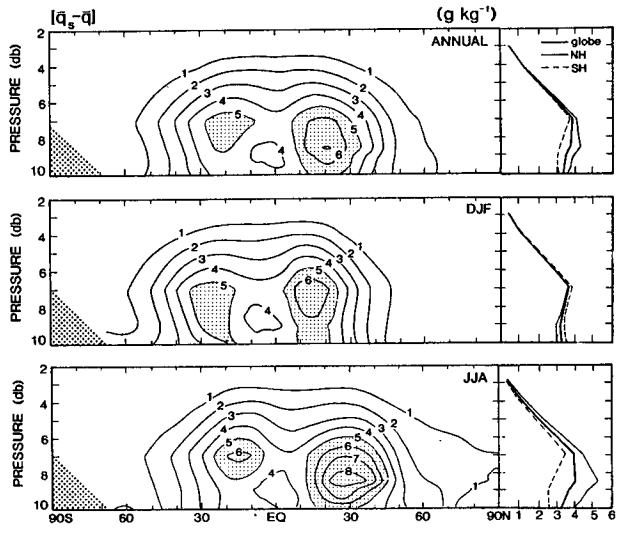

FIG. 6. Zonal mean cross sections of the saturation deficit $(\bar{q} - \bar{q}_s)$ in units of grams per kilogram. Areas where the saturation deficit is larger than 5 g kg^{-1} are shaded.

A simple way of showing the land–sea contrast is to compute the difference of the average relative humidities over ocean and land as presented in Fig. 7. It is interesting to see that in the lower atmosphere (up to 700 mb), the differences are positive in both hemispheres and that they tend to be slightly negative above 700 mb. The highest positive values occur over the Northern Hemisphere with a maximum on the order of 20% in winter and 15% in summer, whereas in the Southern Hemisphere the maximum values are 15% in winter and 10% in summer. The lower values in the Southern Hemisphere compared to those in the Northern Hemisphere are a consequence of the larger extent of the oceans in that hemisphere and less land–sea contrast.

The negative values observed above 700 mb are related to topography or associated with the deeper penetration of moisture over land than over the oceans. This is still more apparent when we see that the highest values occur during summer at about 20°N latitude with strong convection associated mainly with the Asian monsoon. In the Southern Hemisphere the negative values are less extensive and weaker.

To get a better feeling for the three-dimensional variability in relative humidity, annual, summer, and winter cross sections were constructed at various latitudes. These cross sections show the spatial variability, bringing out some special features of the fields. They are presented in Figs. 8–10. The ocean and land influences are clearly shown at 45°N, 30°N, 15°S, and 30°S with minima in the lower troposphere over the continents. The equatorial regions are always moist, whereas at 30°N and 30°S the vertical extent of the moist air is the lowest due to subsidence. The monsoon effects are clearly shown in Fig. 10 between 60°E and 180° at 15°

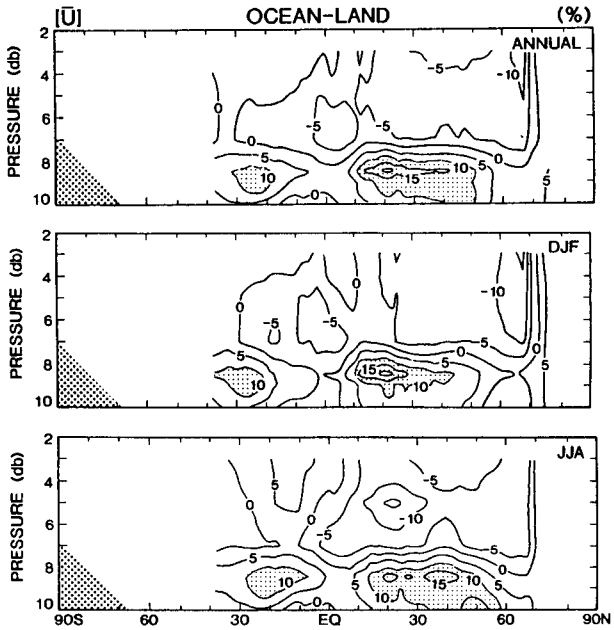

FIG. 7. Vertical cross sections of ocean minus land relative humidity (%). Areas where the differences are larger than 10% are shaded.

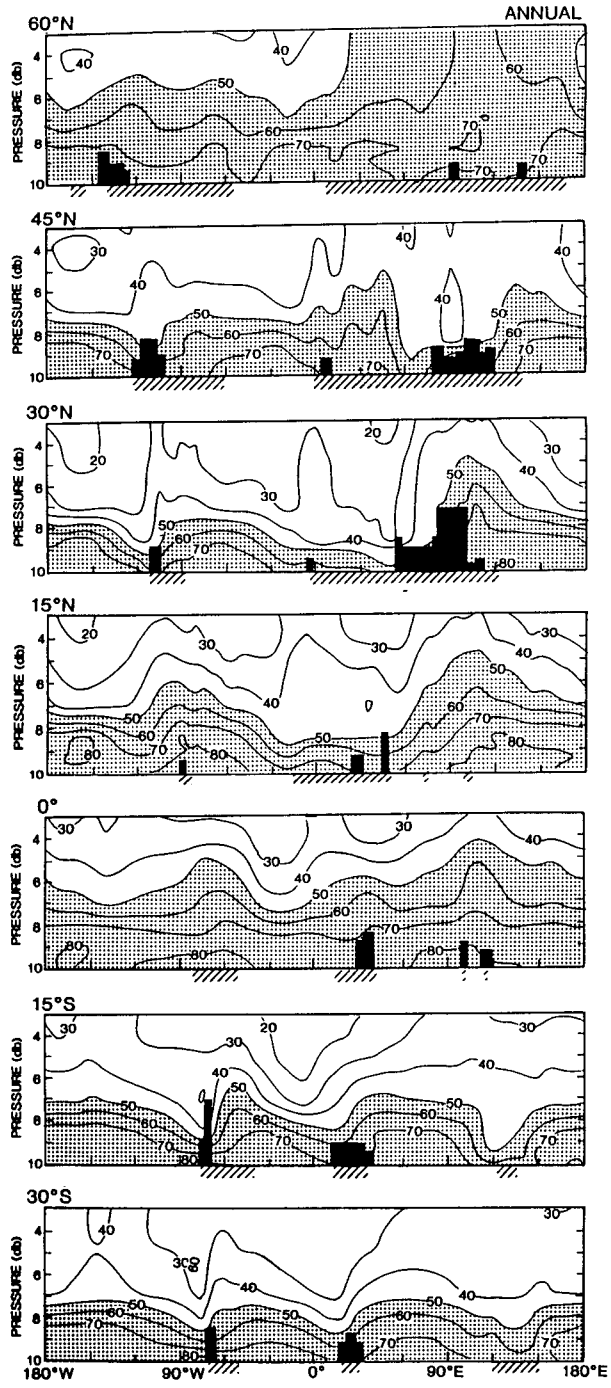

FIG. 8. Longitude–pressure cross sections of the relative humidity (%) at various latitudes for annual conditions. Areas with $\bar{U} > 50\%$ are indicated by heavy shading. The slanted marks at the bottom of each section show the location of the continents. The black areas indicate the major mountain ranges.

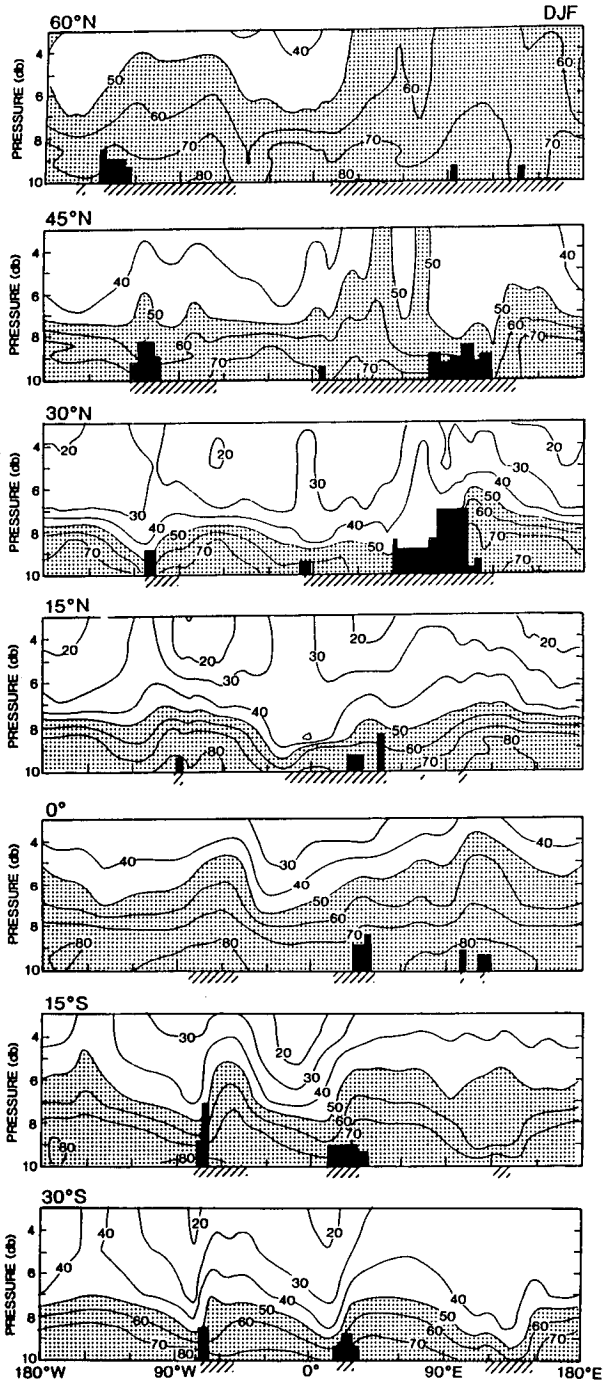

FIG. 9. Longitude–pressure cross sections of the relative humidity (%) between 30°N and 15°S for DJF conditions. Areas with $\bar{U} > 50\%$ are indicated by heavy shading (see also legend Fig. 8).

and 30°N. The deep penetration in summer is also clearly seen over Africa and Central America at 15°N. In the Southern Hemisphere the seasonal effects are not as pronounced. Uniformly high relative humidities are apparent over the high latitudes at 60°N.

In Fig. 11 meridional profiles are presented for oceans and land separately at the 850-mb level where the ocean–land differences are most pronounced (see Fig. 7). As we can see, there is a strong contrast between the profiles for land and sea. The latitudinal variations are more pronounced over the land than over the

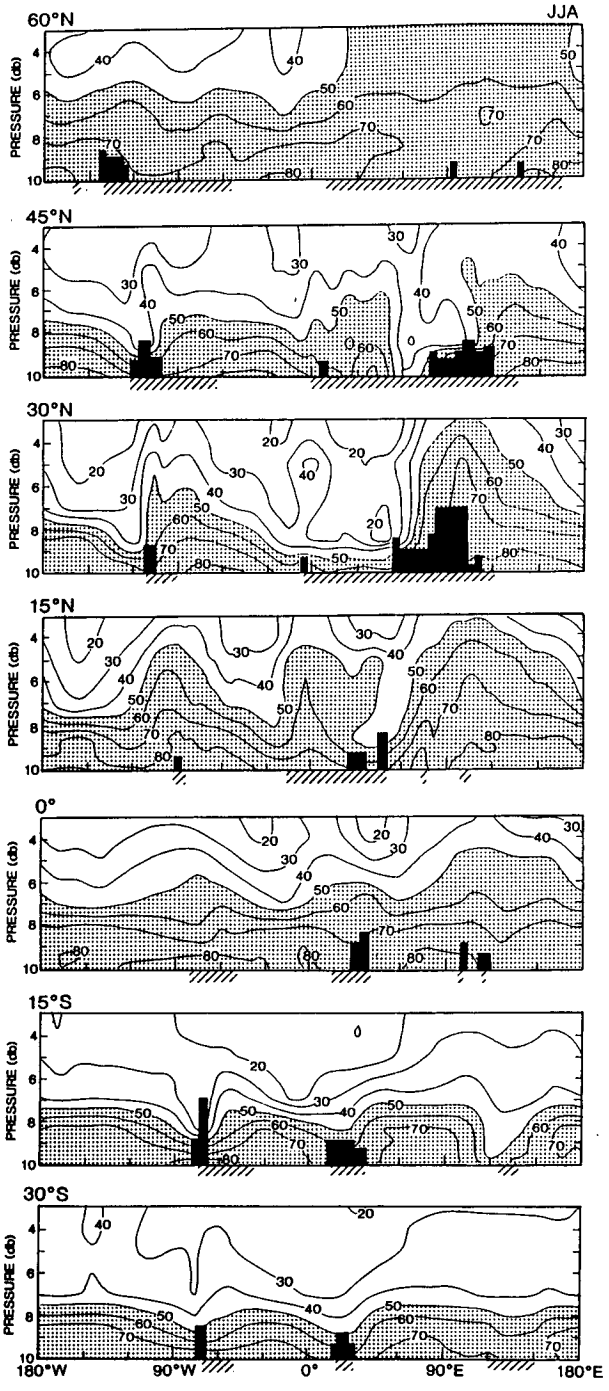

FIG. 10. Same as in Fig. 9 except for JJA conditions.

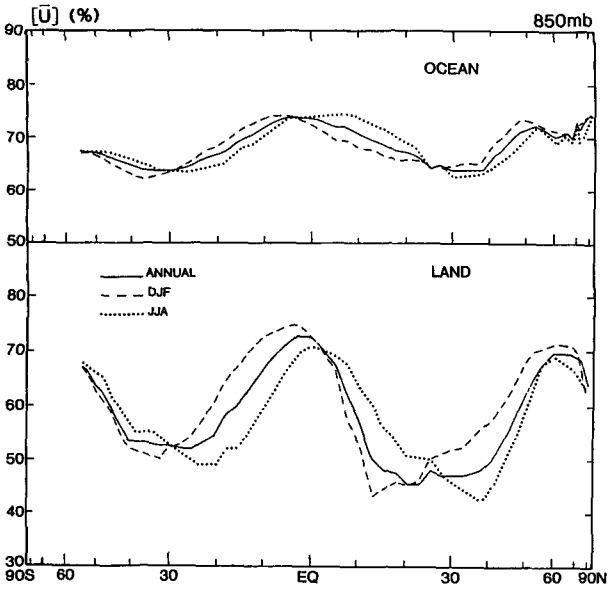

FIG. 11. Meridional profiles of the mean zonal relative humidity (%) at 850 mb for oceans and land.

oceans. The comparison of the profiles for winter and summer shows a much larger seasonal range over the land than over the oceans at the same latitude. The reversal of the seasonal profiles at mid and high latitudes, associated with higher values of relative humidity in the winter season, is best defined at the upper levels, mainly over land (not shown here). The higher relative humidity values over land in winter than in summer may be reinforced by biases of the radiosonde instruments because low humidities are more likely to be missing when the temperatures are low.

Over the continents, the temperature is usually the prevailing factor in determining the relative humidity. This explains why in midlatitudes in the lower troposphere the minimum occurs during the warm season and the maximum during the cold season, except over North America due to the strong summer advection of moist air from the Gulf of Mexico, as discussed above. In the planetary boundary layer the relative humidity over the oceans is more uniform with a small interseasonal and latitudinal variation.

d. Variability in time

As a measure of the stability of our relative humidity values and a possible overall trend in relative humidity during the 1974–88 period, three consecutive 5-yr anomaly values are presented in Table 3 as a function of latitude and pressure. The anomalies are variable and on the order of 1%–2% at the lower levels. However, at the upper levels, especially at 300 mb, the anomalies become larger and more systematic reaching values on the order of ±5%. Most noticeable is the apparent drying out at high latitudes. These downward trends at 300 mb at high latitudes are certainly too large to be real and are probably associated with the general improvement of the radiosondes, usually leading to dryer values (Elliott et al. 1994). However, the smaller decreases at 700 and 500 mb may be an indication of real changes in the relative humidity (see also Oort 1993 and 1994).

The interseasonal variability was already analyzed so that the discussion here will be confined mainly to the day to day variability. This variability is measured by the standard deviation derived from the time series of relative humidity at the different levels $[(\overline{U^2} - \bar{U}^2)^{1/2} = (\overline{U'^2})^{1/2}]$. It is true that the standard deviation also includes the part of the variability associated with the normal seasonal cycle, but the seasonal variability is much smaller than the day to day variability. As mentioned before, the standard deviations for the seasons were computed independently using the mean seasonal values of relative humidity $\bar{U}$ as the reference values. The yearly values were computed with respect to the mean annual value of relative humidity, so that they include also the contributions of the seasonal cycle. In general, we find that the fluctuations for the year are larger than those for the seasons, which explains why the yearly values do not have to lie in between the seasonal estimates.

To characterize the variations, cross sections of the day to day (transient eddy) standard deviations were constructed. The results are shown in Fig. 12. The range of the fluctuations is very large since it is characterized by the alternation of different air masses mainly in mid- to high latitudes. The lowest variability occurs mainly in the equatorial regions and it increases with latitude reaching a maximum on the order of 26% at 700 mb in midlatitudes. The relative humidity variations generally increase with height in the lower troposphere up to the 700-mb level and decrease above that level. The seasonal patterns do not differ much from the annual pattern but are slightly shifted toward the summer pole, and they are somewhat more intense during the winter season, mainly above the planetary boundary layer. The vertical profiles of $(\overline{U'^2})^{1/2}$ in Fig. 12 show an almost parabolic distribution with a flat maximum in the midtroposphere. It is interesting to note that near the earth's surface the variability is relatively small.

The spatial variability is shown in Fig. 13 in terms of the east–west, stationary eddy standard deviations, $[\bar{U} - [\bar{U}]^2]^{1/2} = [\bar{U}^{*2}]^{1/2}$. These stationary eddy variations are less pronounced than the transient eddy ones with maxima on the order of 15% in the subtropics near the 850-mb level. They do not change substantially from one season to another. The vertical profiles show a low tropospheric maximum near 850 mb, and larger values in the Northern Hemisphere associated with the greater land–sea contrasts in that hemisphere.

5. Comparisons

To confirm our results we performed several comparisons resorting directly to the different sources of

TABLE 3. Change in zonal-mean relative humidity (in %) with time for different latitudes and pressure levels. At each pressure level, the first column gives the 1974–88 mean value, and the next three columns give the 5-yr mean anomalies from the 15-yr mean. A clear drying out tendency is found at the upper levels and at high latitudes.

	1000 mb				850 mb				700 mb				500 mb				300 mb			
Latitude	1974–88	74–78	79–83	84–88	1974–88	74–78	79–83	84–88	1974–88	74–78	79–83	84–88	1974–88	74–78	79–83	84–88	1974–88	74–78	79–83	84–88
75.0	78.2	1.1	−0.1	−1.0	69.0	1.2	−0.8	−0.4	60.1	1.3	−0.9	−0.3	52.5	1.5	−0.9	−0.7	50.1	5.0	−1.0	−4.0
60.0	74.4	0.1	0.1	−0.2	69.9	−0.2	0.2	0.0	59.4	0.0	−0.3	0.2	50.1	0.3	−0.3	0.1	47.5	2.2	−0.6	−1.6
45.0	70.9	0.1	0.4	−0.6	58.0	0.1	0.0	−0.1	44.2	0.1	−0.2	0.1	37.0	0.2	−0.3	0.1	34.7	1.1	−0.6	−0.6
30.0	72.3	−0.4	0.6	−0.2	56.8	1.6	−0.4	−1.2	38.7	1.2	−0.6	−0.5	30.3	1.5	−0.8	−0.7	25.5	0.9	−1.0	0.1
15.0	79.6	−1.5	0.5	1.0	68.3	−0.7	0.0	0.8	50.7	−0.5	−0.2	0.7	39.2	0.1	−0.8	0.6	28.6	0.3	−0.4	0.1
0.0	80.1	−0.7	0.0	0.7	74.1	−0.9	−0.3	1.2	55.5	−0.4	−0.7	1.1	42.4	0.3	−1.0	0.7	29.6	1.3	−0.3	−1.1
−15.0	73.8	0.1	−0.4	0.3	63.0	0.4	−0.4	0.0	42.8	2.0	−1.3	−0.7	31.2	3.2	−0.8	−2.4	25.3	4.5	−0.3	−4.3
−30.0	74.4	1.1	−0.9	−0.1	61.1	1.4	−1.3	0.0	38.8	3.0	−1.5	−1.5	31.7	3.6	−1.1	−2.6	29.0	6.4	−0.9	−5.5
−45.0	76.6	2.3	−1.1	−1.2	66.4	0.9	−0.2	−0.6	47.5	2.0	0.0	−2.1	41.7	2.8	0.4	−3.2	37.5	6.2	0.9	−7.1
−60.0	77.9	2.3	−0.9	−1.4	64.6	−0.8	0.2	0.6	55.9	0.0	0.4	−0.4	49.9	0.7	1.4	−2.2	48.3	2.0	3.6	−5.7

humidity data and indirectly to the cloud distributions at different levels.

At the upper levels we used the satellite observations of SAGE for the period 1985–89 to obtain an independent analysis of the distribution of relative humidity.

It is also of interest to compare our results based on the radiosonde network with those obtained from operational analyses such as those given by the ECMWF. We note that besides the radiosonde data other data sources, such as satellite-derived winds and temperatures, are included as input that indirectly affect the ECMWF analyses of humidity. We have chosen to use the ECMWF products because they are generally accepted as one of the best analyses available. Nevertheless, also these analyses are somewhat biased by the (partially) model-derived first-guess field, especially in data-sparse regions (Trenberth and Guillemot 1995).

Finally, in view of the obvious connection between the moisture distribution in the atmosphere and cloudiness, we will use a published climatology for various types of clouds to find out how consistent our results are with the observed cloudiness.

a. Comparisons with SAGE data

To make the radiosonde results compatible with those of the satellite data a subset of our data for the common period 1985–89 was extracted and used to compute the mean relative humidity at the 500- and 300-mb levels. The corresponding profiles at 300 mb are shown in Fig. 14 for the SAGE and radiosonde data. Detailed information on the SAGE data can be found in, for example, Larsen et al. (1993) and Rind et al. (1993). In general, the SAGE data show a drier atmosphere. This is to be expected since there is a bias in the SAGE data toward clear skies, which is especially serious in the equatorial regions where clouds and high moisture are abundant. Furthermore, the radiosonde profiles show a larger seasonal variability than those of SAGE. We intercompared also the results at 500 mb but the SAGE data for this level are not reliable enough to make a detailed comparison with the radiosondes.

In summary, when only the reliable values for SAGE (i.e., those based on a sufficient number of observations) are taken into consideration and are compared with the radiosonde values, one sees that the differences at 300 mb between the zonal means are on the order of 10% in the Tropics and 20% in the high latitudes. We conclude that even at these high levels the radiosonde humidity data are useful, although not accurate enough for estimating trends.

We should note that the radiosonde values at high latitudes presented here are somewhat lower than those shown earlier in Fig. 4. The reason is that in Fig. 14 only the later years are included in the comparisons when the estimates were dryer (see Table 3).

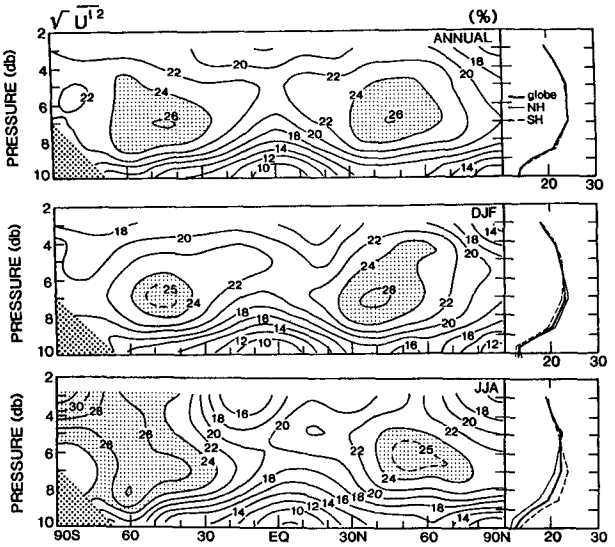

FIG. 12. Cross sections of the zonal mean transient eddy standard deviation of relative humidity in %. Areas with $(\overline{U'^2})^{1/2} > 24\%$ are shaded.

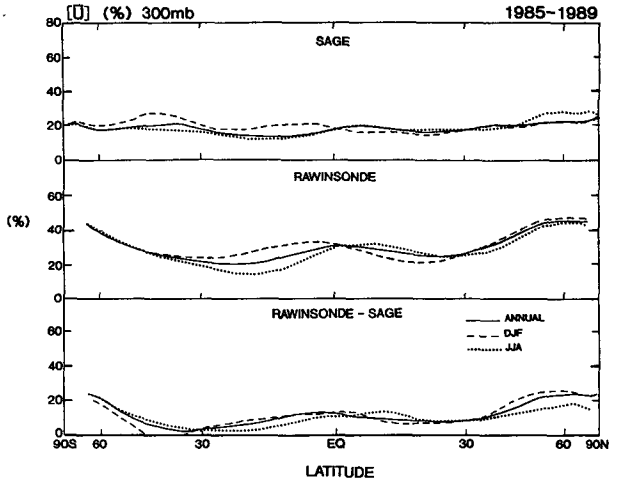

FIG. 14. Meridional profiles of the zonal mean relative humidity (%) for SAGE (top), radiosonde (middle), and the difference (bottom) at the 300-mb level.

b. *ECMWF comparisons*

As a further test of our relative humidity analyses, we have cross validated them with the analyses by the ECMWF. Thus we prepared cross sections of relative humidity using the ECMWF operational analyses for the period 1986–89 (Trenberth and Olson 1988) and compared them with the equivalent cross sections (using the same years) based on the rawinsonde data.

The two sets of analyses given in Fig. 15 show good agreement in the tropical regions where the differences generally do not exceed ±5%. However, the discrepancies are large in the upper troposphere over much of the Tropics and at all levels in the southern extratropics. The ECMWF analyses are more humid in mid to high latitudes at upper levels and, in general, in the Southern Hemisphere, but they tend to be lower than the radiosonde analyses in the Tropics in the midtroposphere. This suggests that perhaps in the ECMWF model–observations assimilation scheme the mechanisms for the vertical transport of moisture are not strong enough to generate sufficient penetrative convection and that the ECMWF Hadley cells may have a weaker intensity. The differences between the two analyses are compa-

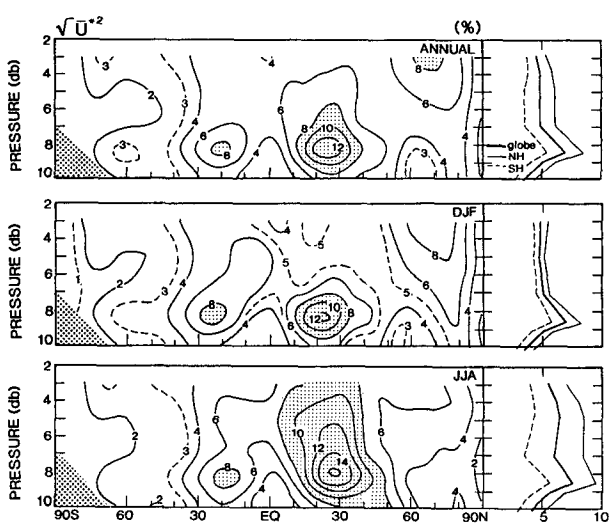

FIG. 13. Same as in Fig. 12 except for stationary eddies. Areas with $(\bar{u}^{*2})^{1/2} > 8\%$ are shaded.

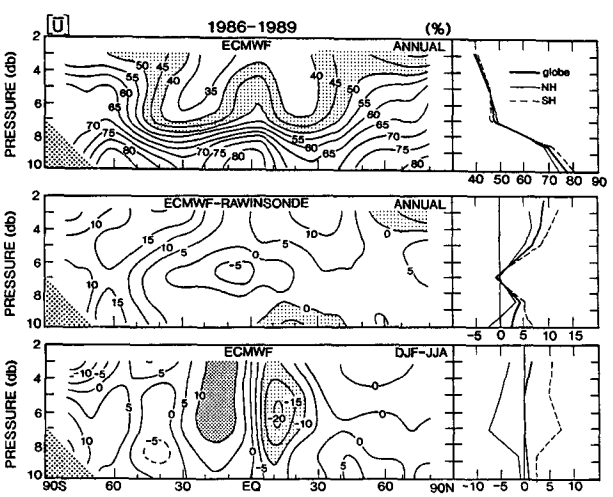

FIG. 15. Mean annual cross sections of the relative humidity (%) as given by the ECMWF analyses (top), the difference ECMWF-radiosonde (middle), and the seasonal variability (bottom) for the ECMWF analyses.

rable to or even larger than the seasonal differences poleward of 30° latitude.

A cross section for the seasonal variation of the ECMWF analyses is shown at the bottom of Fig. 15. In the Tropics, it does not differ by more than 5% from the corresponding radiosonde-based cross section (Fig. 4), but it is less intense in the Southern Hemisphere. The hemispheric averages show a less smooth, probably less realistic vertical profile than in the pure radiosonde case in Fig. 4. However, the seasonal range profiles are very similar.

c. *Comparisons with cloudiness*

The current knowledge of the cloud climatology is still limited and, in some respects, not adequate. Among the difficulties involved we can mention that the cloud heights are inferred from surface observations: clouds in one layer obscure the clouds above, the vertical extent of clouds is difficult to assess, etc. Furthermore, the clouds classification is qualitative and depends to some extent on the observer. The middle clouds can be observed less frequently than low clouds, and high clouds even less. In spite of these difficulties, the main cloudiness features are well observed as far as climatological studies are concerned (Hahn et al. 1982, 1984). In the early 1980s, the International Satellite Cloud Climatology Project (ISCCP) was launched to obtain more detailed global information on clouds and to improve the overall quality of the cloud data.

Several huge efforts have been made to construct global distributions of the various types of clouds. From these studies, we chose to use the cloud data produced by Hahn et al. (1982, 1984) for comparison with our results for relative humidity. However, we should not expect a very strong correlation on physical grounds between clouds and relative humidity since besides relative humidity other dynamical factors, such as vertical motions, also regulate cloud formation. On the other hand, inside clouds there is saturation with values of 100% relative humidity. We may note that recent work by Lau and Crane (1995; 1996, personal communication) showed excellent agreement between the ISCCP-derived and surface cloud estimates, even on a synoptic scale (except for low clouds that cannot be seen by satellite when higher-level clouds are present).

To simplify the comparisons in the present study, low clouds were assigned to the 850-mb level, mid clouds to 700 mb, and high clouds to 500 mb. With the two-dimensional fields provided by Hahn et al., mean zonal profiles were constructed for high, mid-, and low clouds for annual and seasonal conditions.

The profiles thus obtained are shown in Fig. 16. They show similar latitudinal variations compared to the values for relative humidity shown in the cross sections in Figs. 4 and 11. The relative maximum at 5°N evident

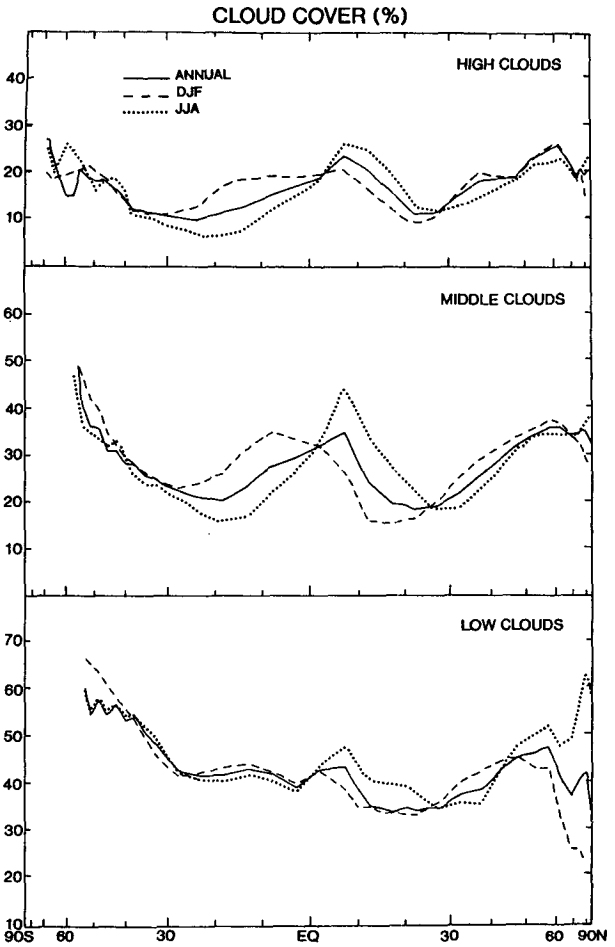

FIG. 16. Meridional profiles of the zonal mean cloud cover (%) for high, mid, and low clouds.

in all profiles is due to enhanced convection in the rising branches of the Hadley cells. The minima in the subtropics due to subsidence associated with the subtropical high pressure belts can be detected in the figures at all levels. In fact, the downward motion inhibits the formation of clouds due to adiabatic heating. At high latitudes cloudiness increases again for all types of clouds.

The distributions of cloudiness and relative humidity are almost symmetrical with respect to the equator, except for low clouds. The shapes of the low cloud profiles between 30°N and 30°S are similar to those of $[\bar{U}]$ and reveal some interhemispheric asymmetries. The values in the Northern Hemisphere are lower than in the Southern Hemisphere associated with the existence of extensive desert regions in the Northern Hemisphere where clear skies prevail. Over the oceans at the same latitudes small cumulus or stratocumulus always develop, which also explains some of the interhemispheric asymmetries and the differences in seasonal amplitudes. The larger low and midcloud coverage in

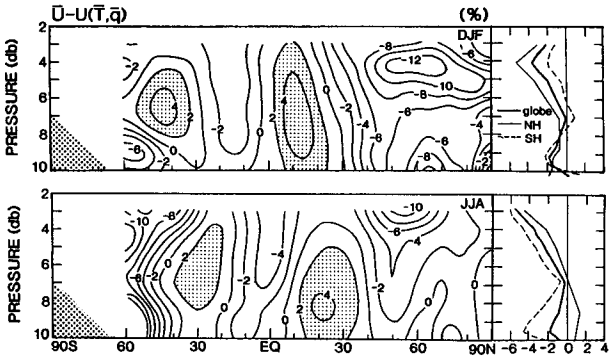

FIG. 17. Cross sections of the difference of the mean relative humidity (%) computed from the daily relative humidity data and of the relative humidity computed from the time-mean temperature and time-mean specific humidity for DJF and JJA. Areas with differences greater than 2% are shaded.

the Southern Hemisphere around Antarctica is associated with the higher activity of depressions compared with the same latitudes in the Northern Hemisphere.

6. Concluding remarks

We will now pass in review some aspects of the potential of relative humidity measurements from satellites. Satellite information is a very important new source of data for the upper troposphere and stratosphere. For the midtroposphere, however, the satellite soundings are less useful because they stop at cloud tops, so that no data are available below clouds. Other shortcomings lie in the poor vertical resolution of the satellite soundings. This resolution is typically of the order of several kilometers, which is a very coarse resolution for the troposphere (e.g., Rind et al. 1993).

Satellite data, however, give a much more uniform spatial coverage allowing, in some cases, a scrutiny of the inhomogeneity of the radiosonde network. Satellite observations can even constitute a reference basis for comparison of various types of radiosondes as shown by Soden and Lanzante (1996). In this study, they used radiation measurements in certain infrared channels (6.7-, 7.3-, and 8.3-μm channels) to infer the relative humidity for the upper, mid-, and lower tropospheric layers. In comparing their results with the radiosonde network, they found that at high levels, the eastern European and Asian radiosondes (type A) gave higher values (>10%), whereas the western and Southern Hemisphere radiosondes (type B) gave lower average values ($\sim -10\%$). These differences were attributed to the different types of sensors used. The goldbeaters' skin used in most type A radiosondes gives higher estimates than the others due to the longer lag, mainly at the higher levels. However, the discrepancies between the two radiosonde types become much smaller in the mid- and lower troposphere.

In trying to assess the effects of spatial sampling on the radiosonde climatology, Soden and Lanzante (1996) found some discrepancies, mainly in the regions of poor data coverage such as the South Indian Ocean and the eastern equatorial Pacific. Similar findings were reported by Raval et al. (1994) in the case of the distribution of precipitable water when they compared the Special Sensor Microwave/Images (SSM/I) satellite analyses with those obtained from the rawinsonde network.

Let us now return to the discrepancies involved in the two approaches to compute the mean relative humidity as described in section 3d. The differences $\bar{U} - \bar{U}^{\dagger}$ can be either positive or negative [see expression (23)]. These discrepancies can be substantial at individual locations and even for some regional averages over the globe. To assess these differences for the globe, $\bar{U} - \bar{U}^{\dagger}$ fields were constructed for seasonal and annual mean conditions (not presented here). These fields show consistent negative difference patterns in the high-latitude regions and positive patterns in the tropical regions. The general features can be detected in Fig. 17, which gives cross sections of the mean zonal values $[\bar{U} - \bar{U}^{\dagger}]$ for both extreme seasons obtained from the horizontal analyses. The cross sections show alternating positive and negative latitudinal centers of the same order of magnitude, with extreme values of about 10%. These centers shift with the seasons. As far as the hemispheric-mean vertical profiles in Fig. 17 are concerned, we see that the differences between the two methods are relatively minor.

As expression (23) shows, the minus sign stems from the covariance signal of $\overline{q'q'_s}$. Since q_s is only a function of T, we can make our analyses using the transient eddy covariance $\overline{q'T'}$ instead. The horizontal fields of $\overline{q'T'}$ were analyzed previously but will not be given here. We will only show the final cross sections of the mean zonal values $[\overline{q'T'}]$ (see Fig. 18). The values are positive in the mid- to high latitudes and

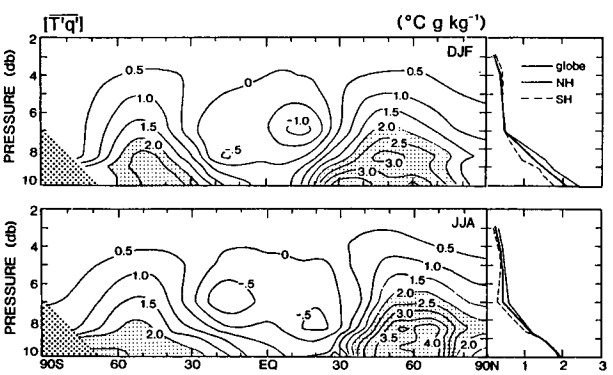

FIG. 18. Zonal mean cross sections of the temporal covariance of the temperature and specific humidity (°C g kg^{-1}) for DJF and JJA. Areas greater than 2.0°C g kg^{-1} are shaded.

slightly negative over the intertropical regions. Thus, assuming that the $\overline{q'T'}$ and $\overline{q'q'_s}$ have similar patterns and equivalent intensities, they give, being negative, a positive contribution in the Tropics, reinforcing the already positive character of $[\bar{U} - \bar{U}^{\dagger}]$. On the other hand, when $\overline{q'T'}$ is positive and sufficiently large, the minus sign for $\bar{U} - \bar{U}^{\dagger}$ will prevail leading to the negative $[\bar{U} - \bar{U}^{\dagger}]$ values in high latitudes.

The fields of $\overline{q'T'}$ have their own intrinsic importance. In general, warm air masses are associated with high moisture content and cold air masses with low moisture content in mid- and high latitudes due to advection ($\overline{q'T'} > 0$). However, subsidence in the subtropical anticyclones, convection in the equatorial belt, and advection of warm and dry continental air masses can lead to negative covariance values of $\overline{q'T'}$ over the tropical regions. Thus, over the equatorial and subtropical regions a well-defined area of negative $\overline{q'T'}$ values is found above the surface. The most intense centers are related to subsidence (compare Fig. 4), whereas the equatorial belt values must be related to condensation and precipitation. In this last case, $\overline{q'T'}$ [see expression (18)] is related to strong condensation (precipitation) associated with rising vertical motions with an equivalent release of latent heat of $-Lq'$. Since the generation of available potential energy is given by $G(P) = \int \Gamma \overline{Q'T'}$ (Peixoto and Oort 1992, section 14.3), where Q is the diabatic heating rate and Γ a measure of the static stability, we see that when condensation occurs, the generation due to the release of latent heat can be written as

$$G(P) = -\int \Gamma L \overline{q'T'} dm \qquad (24)$$

(see Peixoto 1965). Thus, in the equatorial regions there is a positive generation of available potential energy associated with condensation.

The vertical profiles at the right-hand side of Fig. 18 show clearly the strongest covariance values near the earth surface, where the variations of q are also the strongest.

Finally, we will summarize some of the major results of the present study.

1) For the first time, a comprehensive, three-dimensional description of the global climatology of relative humidity is presented based on 15 years of data from more than 1000 radiosonde stations.

2) The strengths and weaknesses of the humidity measurements are clearly shown (sections 1 and 3).

3) A thorough theoretical analysis is presented of the relationships between the variations in temperature, dewpoint temperature, and specific humidity and those in relative humidity (section 2).

4) We find a high degree of variability in space and time of the observed relative humidity (section 4), in contrast with some GCM simulations that show the tendency for a more constant relative humidity (sections 1 and 5c).

5) Extensive comparisons of the rawinsonde-derived climatology with other analyses, such as from satellite data (SAGE), surface cloud data, and operational analyses (ECMWF), are given (section 5).

6) As a by-product of the theoretical analyses, zonal-mean cross sections of the $\overline{q'T'}$ covariance are shown, which are also important in the study of the release of latent heat.

Acknowledgments. The authors would like to thank Jerry Mahlman, the Director of GFDL, for his support of our joint research; John Lanzante, Leo Donner, and the official reviewers for reviewing our manuscript and giving many helpful suggestions that have led to significant improvements in the original manuscript; Mel Rosenstein and Mark Crane for programming support; Par Suntharalingam for preparing the SAGE data; Kevin Trenberth for providing the ECMWF analyses; Carole Hahn of CIRES/Boulder for help with the cloud data; Jeff Varanyak and Catherine Raphael for drafting the figures; and Wendy Marshall for typing the manuscript.

REFERENCES

Elliott, W. P., and D. J. Gaffen, 1991: On the utility of radiosonde humidity archives for climate studies. *Bull. Amer. Meteor. Soc.*, **72,** 1507–1519.

——, ——, J. D. W. Kahl, and J. K. Angell, 1994: The effect of moisture on layer thicknesses used to monitor global temperatures. *J. Climate,* **7,** 304–308.

Emanuel, K. A., 1994: *Atmospheric Convection.* Oxford University Press, 580 pp.

Gaffen, D. J., 1993: Historical changes in radiosonde instruments and practices. World Meteorological Organization/TD-No. 541, Rep. 50, 123 pp. [Available from World Meteor. Org., Case Postale No. 2300, CH-1121, Geneva 2, Switzerland.]

——, A. Robock, and W. P. Elliott, 1992: Annual cycles of tropospheric water vapor. *J. Geophys. Res.,* **97,** 18 185–18 193.

Hahn, C. J., S. G. Warren, J. London, R. M. Chervin, and R. Jenne, 1982: Atlas of simultaneous occurrence of different cloud types over the ocean. NCAR/TN-201 + STR, 212 pp. [Available from author at CIRES, Campus Box 449, University of Colorado, Boulder, CO 80309.]

——, ——, ——, ——, and ——, 1984: Atlas of simultaneous occurrence of different cloud types over land. NCAR/TN-241 + STR, 21 pp. and 47 maps. [Available from author at CIRES, Campus Box 449, University of Colorado, Boulder, CO 80309.]

Harris, R. G., A. Thomasell Jr., and J. G. Welsh, 1966: Studies of techniques for the analysis and prediction of temperature in the ocean, part III: Automated analysis and prediction. Interim Report, prepared by Travelers Research Center, Inc., for U.S. Naval Oceanographic Office, Contract #N62306-1675, 97 pp. [Available from A. H. Oort, GFDL/NOAA, P.O. Box 308, Princeton, NJ 05842.]

Haurwitz, B., and J. M. Austin, 1944: *Climatology.* McGraw-Hill, 410 pp.

Iribarne, J. V., and W. L. Godson, 1973: *Atmospheric Thermodynamics.* D. Reidel, 222 pp.

Lanzante, J. R., 1996: Resistant, robust and nonparametric techniques for the analysis of climate data: Theory and examples, including applications to historical radiosonde station data. *Int. J. Climatol.,* in press.

Larsen, J. C., E. W. Chiou, W. P. Chu, M. P. McCormick, L. R. McMaster, S. Oltmans, and D. Rind, 1993: A comparison of the stratospheric aerosol and gas experiment II tropospheric water vapor to radiosonde measurements. *J. Geophys. Res.*, **98,** 4897–4917.

Lau, N. C., and M. W. Crane, 1995: A satellite view of the synoptic-scale organization of cloud properties in midlatitude and tropical circulation systems. *Mon. Wea. Rev.*, **123,** 1984–2006.

Levitus, S., 1982: *Climatological Atlas of the World Ocean.* NOAA Prof. Paper No. 13, U.S. Government Printing Office, Washington, D.C., 173 pp.

Manabe, S., and R. T. Wetherald, 1967: Thermal equilibrium of the atmosphere with a given distribution of relative humidity. *J. Atmos. Sci.*, **24,** 241–259.

——, and ——, 1975: The effects of doubling the CO_2-concentration on a general circulation model. *J. Atmos. Sci.*, **32,** 3–15.

Mitchell, J. F. B., and W. J. Ingram, 1992: Carbon dioxide and climate: Mechanisms of changes in cloud. *J. Climate,* **5,** 5–21.

Nash, J., and F. J. Schmidlin, 1987: WMO International Radiosonde Intercomparison. Final Rep. WMO/TD-No. 195, World Meteor. Org., Instruments and Observing Methods Rep. 30, 103 pp. [Available from World Meteor. Org., Case Postale No. 2300, CH-1121, Geneva 2, Switzerland.]

Oort, A. H., 1983: Global atmospheric circulation statistics, 1958–1973. NOAA Prof. Paper 14, 180 pp. and 47 microfiche. [Available from author at GFDL/NOAA, P.O. Box 308, Princeton, NJ 08542.]

——, 1993: Observed humidity trends in the atmosphere. Preprints, *Proc., 17th Annual Climate Diagnostics Workshop,* Norman, OK, Amer. Meteor. Soc., 24–30.

——, 1994: An investigation of the historical station records of upper air humidity. Preprints, *Proc., 18th Annual Climate Diagnostics Workshop,* Boulder, CO, Amer. Meteor. Soc., 346–351.

——, and J. J. Yienger, 1996: Observed variability in the Hadley circulation and its connection with ENSO. *J. Climate,* **9,** 2751–2767.

Pan, Y. H., and A. H. Oort, 1983: Global climate variations connected with sea surface temperature anomalies in the Eastern Equatorial Pacific Ocean for the 1958–73 period. *Mon. Wea. Rev.*, **111,** 1244–1258.

Peixoto, J. P., 1965: On the role of water vapor in the energetics of the general circulation of the atmosphere. *Port. Phys.*, **4,** 135–170.

——, and A. H. Oort, 1983: The atmospheric branch of the hydrological cycle and climate. *Variations in the Global Water Budget,* A. Street-Perrott, et al. Ed., Reidel, 5–65.

——, and ——, 1992: *Physics of Climate.* American Institute of Physics, 520 pp.

Rasmusson, E. M., 1967: Atmospheric water vapor transport and the water balance of North America. Part 1. Characteristics of the water vapor flux field. *Mon. Wea. Rev.*, **95,** 403–426.

——, 1972: *Seasonal Variation of Tropical Humidity Parameters.* Vol. 1, *The General Circulation of the Tropical Atmosphere,* R. E. Newell et al., Eds., The MIT Press, 258 pp.

Raval, A., A. H. Oort, and V. Ramaswamy, 1994: Observed dependence of outgoing longwave radiation on sea surface temperature and moisture. *J. Climate,* **7,** 807–821.

Rind, D., E.-W. Chiou, W. Chu, J. Larsen, S. Oltmans, J. Lerner, M. P. McCormick, and L. McMaster, 1991: Positive water vapor feedback in climate models confirmed by satellite data. *Nature,* **349,** 500–503.

——, ——, ——, S. Oltmans, J. Lerner, J. Larsen, M. P. McCormick, and L. McMaster, 1993: Overview of the stratospheric aerosol and gas experiment II water vapor observations: Method, validation, and data characteristics. *J. Geophys. Res.*, **98,** 4835–4856.

Saucier, W. J., 1955: *Principles of Meteorological Analysis.* University of Chicago Press, 438 pp.

Soden, B. J., and J. R. Lanzante, 1996: An assessment of satellite and radiosonde climatologies of upper tropospheric water vapor. *J. Climate,* **9,** 1235–1250.

Spiegel, M. R., 1961: *Statistics—Schaums's Outline Series in Mathematics.* McGraw Hill, 359 pp.

Starr, V. P., J. P. Peixoto, and G. C. Livadas, 1958: On the meridional flux of water vapor in the Northern Hemisphere. *Geofis. Pura Appl.,* **39,** 174–185.

Sun, D.-Z., and A. H. Oort, 1995: Humidity-temperature relationships in the tropical troposphere. *J. Climate,* **8,** 1974–1987.

——, and I. M. Held, 1996: A comparison of modeled and observed relationships between interannual variations of water vapor and temperature. *J. Climate,* **9,** 665–675.

Szava-Kovats, J., 1938: Verteilung der Luftfeugtigkeit auf die Erde. *Ann. Hydrogr.,* **66,** 373–378.

Telegadas, K., and J. London, 1954: Physical model of the Northern Hemisphere Troposphere for winter and summer. New York University, Scientific Report No. 1, AF 19(122)-165, 55 pp. [Available from J. London, Dept. of Astrophysical, Planetary and Atmospheric Sciences, University of Colorado, Boulder, CO 80309.]

Tetens, O., 1930: Ueber einige meteorologische Begriffe. *Z. Geophys.,* **6,** 297–309.

Trenberth, K. E., and J. G. Olson, 1988: ECMWF global analyses 1979–1986: Circulation statistics and data evaluation. NCAR/TN-300 + STR, 94 pp. [Available from author at Climate Analysis Section, NCAR, ML, P.O. Box 3000, Boulder, CO 80307.]

——, and C. J. Guillemot, 1995: Evaluation of the global atmospheric moisture budget as seen from analyses. *J. Climate,* **8,** 2255–2272.

WMO (World Meteorological Organization), 1983: Guide to Meteorological Instruments and Methods of Observation. Fifth Edition, WMO-No. 8, 13.1–13.26 pp. [Available from World Meteor. Org., Case Postale No. 2300, CH 1121, Geneva 2, Switzerland.]

Woodruff, S. D., R. J. Slutz, R. L. Jenne, and P. M. Steurer, 1987: A Comprehensive Ocean–Atmosphere Data Set. *Bull. Amer. Meteor. Soc.,* **68,** 1239–1250.